Actuators Displaying Unidirectional Movement

Mridula Nandi, Binoy Maiti, and David Díaz Díaz*

Shape memory polymer actuators have attracted great attention in the past few decades for developing soft robots, artificial muscles, and biomedical implants, among others. Herein, under a tutorial perspective, a series of shape memory actuators that display unidirectional movement upon exposure to specific external stimuli is explored. The mechanistic details associated with the movement of each system are also highlighted. In general, an overview of basic design principles, the chemical structure of molecular switches, the strategies used to achieve such controlled and unidirectional movement, as well as key experimental aspects, is provided. The most critical challenges of the existing devices that limit their practical applicability are also discussed. This is of utmost importance because such limitations must be overcome to fabricate micromotors that can generate complex movements, other than simple stretching/contraction or bending, to perform complex tasks.

1. Introduction

One of the most fundamental challenges in developing artificial smart materials is to trigger directed motion, which involves interconversion of chemical energy and mechanical energy.[1] Primarily biological systems ranging from unicellular organisms and plants to human beings use anisotropic structures of the basic building units to achieve complex motions in response to environmental conditions.[2] Inspired from nature, scientists have incorporated the concept of anisotropy into synthetic materials to develop intelligent materials with the purpose of mimicking biological systems.[3] Of particular interest are shape memory polymers (SMPs), which belong to a class of smart materials that

can undergo reversible shape deformations upon external stimuli.

Within this context, SMPs can be programmed to memorize a particular shape, undergo a subsequent shape change when subjected to an environmental stimulus and recover the memorized shape when the stimulus is released.[4] The physical information pertaining to the memorized shape is encoded into their molecular structure during the reshaping process, generally termed as programming. Currently, the application of SMPs as biomimetic soft robots,[5] artificial muscles,[6] valves,[7] minimally invasive implants,[8] self-regulating iris,[9] and microswimmers[10] is gaining momentum. Considerable research is being done to investigate the underlying working principles of these materials (e.g., trigger mechanisms of molecular switches), and integrate multishape memory features as well as multiple functions into a single system.[11,12] Typically, energy derived from various external stimuli such as temperature,[13,14] light,[15] pH,[16,17] and electric[18] and magnetic field[19] is exploited to induce the reversible shape transformation in these materials. Among them, temperature is one of the most explored stimuli whereby the shape memory effect is generated due to the thermal phase transitions of the polymers, namely, glass transition and melting temperatures,[20] or due to anisotropic expansion/contraction of hydrogels at the critical solution temperature. In contrast, the use of light as stimulus allows controlling the shape switching precisely and instantly at ambient temperature. In this sense, performing actuation near body temperature is advantageous for SMPs to be used in biomedical applications. For electroresponsive actuators, the electric stimulus can be operated remotely along with controllable field strength, direction, and rapid "on/off" triggering switch. On the other hand, magnetically actuated materials are quite intriguing because they can be operated in many different media, including air, vacuum, and conducting and nonconducting liquids, without having any physical contact with the actuator. More recently, actuators that can respond to multiple stimuli have attracted significant research attention.[21,22] Taking all this into account, the reversible macroscopic movement of an SMP can be translated into an actuating behavior by applying multiple on/off cycles of the external stimuli. Polymeric hydrogels are promising candidates as soft actuators due to their soft, flexible, and open 3D structure, which also makes them generally compatible with biological tissues. The properties of any material are essentially determined by their molecular structures. Therefore, for hydrogel actuator deformation, shape changes, response time, and actuation mainly depend on their inhomogeneous structures. Some of the earliest reports

Dr. M. Nandi, Dr. B. Maiti, Prof. D. Díaz Díaz
Institut für Organische Chemie
Universität Regensburg
Universitätsstr. 31, 93053 Regensburg, Germany
E-mail: David.Diaz@chemie.uni-regensburg.de, ddiazdiaz@ull.edu.es

Prof. D. Díaz Díaz
Departamento de Química Orgánica
Universidad de La Laguna
Avda. Astrofísico Francisco Sánchez, 38206 La Laguna, Tenerife, Spain

Prof. D. Díaz Díaz
Instituto Universitario de Bio-Orgánica Antonio González
Universidad de La Laguna
Avda. Astrofísico Francisco Sánchez 2, 38206 La Laguna, Tenerife, Spain

The ORCID identification number(s) for the author(s) of this article can be found under https://doi.org/10.1002/aisy.202000214.

on shape transformation dealt with cross-linked polymer acids—polymethacrylic and polyacrylic acids (PAAs)—which could swell anisotropically and exhibited reversible dilations/contractions on alternate exposure to acids and alkali, due to the ionizable groups present in the polymer side chains.[23] Specifically, the corresponding cross-linked hydrogels were mechanically strong enough to hold up a load and the reversible dimension changes assisted in lifting and lowering the load.[24] Apart from polymeric hydrogels, liquid crystalline elastomers,[25,26] nanocomposite hydrogels,[27] alloys,[28] and carbon nanotube composites[29] have also been investigated for shape memory actuation.

Particularly for applications in soft robotics, controllable shape deformations such as bending,[30] expansion/contraction,[31] twisting,[32] and gripping[33] are of considerable interest. In this progress report, we review some recent developments in polymeric actuators focusing particularly on those capable of unidirectional movement. In the following sections an analysis of the device fabrication methods, mechanism of energy transformation into mechanical deformation, as well as their main applications is presented based on the nature of the stimuli used. It is much more difficult, rather scientifically challenging, to design materials that exhibit unidirectional movement. Features such as movement speed control and covered distance in unidirectional actuators, which could boost the number of applications of actuators in soft robotics for remote transportation and biomedical devices, are great

challenges to achieve. The number of such examples is still very limited, albeit growing very fast in the last few years, so it is timely to review and highlight what are the strategies that researchers worldwide are exploring to achieve such controlled movement. At this point, it is important to mention that detailed fabrication strategy and actuating behavior of biomimetic actuators displaying other types of movements are described elsewhere and are out of the scope of this contribution.[34,35]

2. Various Stimuli-Responsive Actuators

The ability to sense and respond to environmental conditions is an intrinsic characteristic of some polymeric materials. Typically, the response is generated due to specific functional groups present in the polymer and any change in their properties upon exposure to external stimuli. To design polymeric actuators for specific applications, it is important to select an appropriate material as the bulk performance of the actuator originates from its specific stimuli responsiveness at the molecular level. In the following subsections, we highlight the most relevant systems and discuss their fabrication strategies, actuation mechanism, and the environmental triggers used in each case. **Table 1** summarizes the examples discussed in this contribution along with the required environmental stimuli and key actuation properties.

Table 1. Shape memory soft actuators displaying unidirectional movement, required environmental stimuli, and actuation features.
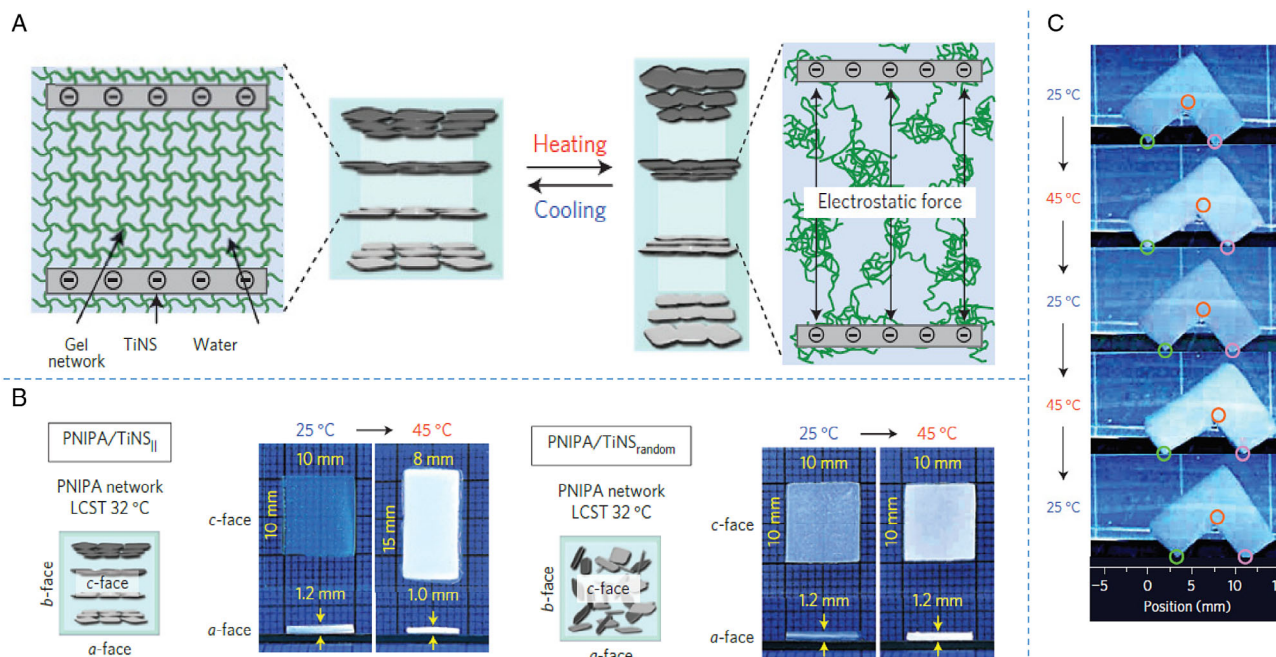
Type of material[a]	External stimuli	Speed of movement	Distance moved [mm]	Deformation (response time)[b]	Reference
PNIPAM hydrogel	Temperature	14.9 μm s^{-1}	–	38% (shrinkage in volume)	[36]
PNIPAM/TiNS$_{\parallel}$ hydrogel	Temperature	–	–	170% (1 s)	[38]
Azobenzene-based LC elastomer	Light	–	–	12–18% (1 min)	[40]
Graft polymer film	Light	–	–	R_f (%): 11–38% R_r (%) > 98%	[42]
IPN film	Light	–	–	R_f (%): 20–33% R_r (%) > 88%	[42]
Multiblock polyesterurethane composed of PCL/PLLA	Light	–	–	R_f (%): 32–55% R_r (%) > 95%	[43]
p(NIPAM-*co*-SP-*co*-AA) hydrogel	Light	–	–	56–62% (contraction) 75–78% (expansion)	[45]
PNIPAM/TiNS$_{\parallel}$/AuNP hydrogel	Light	3.4 mm min^{-1}	7	180% (<0.5 s)	[48]
PAA/PAAm layered hydrogel	Electric field	–	–	10% (1 min)	[52]
PVA/DMSO gel	Electric field	14.4 mm s^{-1}	50	–	[53]
Poly(AMPS-*co*-AAm) hydrogel	Electric field	4.2–8 mm min^{-1}	7.16–13.44	–	[54]
AAm/NaAc and AAm/DMAEMA-Q-based hydrogel	Electric field	≈2.5 mm min^{-1}	–	–	[55]
DOPA-containing peptide-based hydrogel	Electric field	–	–	17.3%[c] 59.5%[d]	[56]
PAH/PAA LbL film	RH	–	–	(2.8–8.0 s)	[59]
CNP film	RH	–	–	(<0.5 s)	[60]
Poly(NIPAM-*co*-Ru(bpy)$_3$-*co*-AMPS)-based hydrogel	BZ reaction	≈170 μm min^{-1}	–	–	[61]

[a]See Appendix for relevant chemical structures; [b]R_f = strain-fixity rate, R_r = strain-recovery rate; [c]See Figure 9D; [d]See Figure 9F. Note: A dash denotes absence of data in the corresponding reference.

ADVANCED
SCIENCE NEWS
www.advancedsciencenews.com

ADVANCED
INTELLIGENT
SYSTEMS
Open Access
www.advintellsyst.com

2.1. Thermoresponsive Actuators

Temperature as an environmental stimulus has long been used to generate actuating behavior in polymers through volume phase transition of the polymeric network. Thermoresponsive polymers can be categorized into two types, those having either lower critical solution temperature (LCST) or upper critical solution temperature (UCST). Hydrogels possessing LCST remain swollen below the LCST and shrink expelling water from the hydrogel matrix when heated above the LCST. Conversely, hydrogels displaying an UCST swell above their UCST. For instance, poly(N-isopropylacrylamide) (PNIPAM), which possesses an LCST of 32 °C was the first thermoresponsive hydrogel to be investigated for bioactuation. By spatial manipulation of the volume phase transition, micromotors can be devised for cargo transport. Based on this theory, Wiesner and coworkers constructed a micromachine from PNIPAM hydrogel, which was capable of moving unidirectionally with a gel velocity of $14.9 \mu m s^{-1}$, for one full cycle of shrinking and swelling of the hydrogel.[36] The experimental setup consisted of a glass tube containing PNIPAM hydrogel connected to a thermoelectric module for heating. Cylindrical PNIPAM gels of length ≈4 cm were synthesized in glass tubes with an inner diameter of 0.7 cm using N,N′-methylenebis(acrylamide) (BIS) as cross-linker agent. To prevent the outer surface of the gels from adhering to the glass surface, the tube was coated with diethoxydimethylsilane (DEDMsilane). The portion of the tube unoccupied by the gel was filled with deionized water and the ends of the tubes were sealed. Then, the tubes were mounted on a series of 9 mm × 9 mm Peltier elements that functioned as heat pumps, regulating the direction of the heat transfer. Each of the Peltier units was controlled discretely by a direct current (DC) power supply through a switch. Starting from one end, heating one or more of the Peltier elements followed by cooling from the same end triggered sequential contraction/expansion of the hydrogel segments along their length, which resulted in propagation of the polymer gel in the forward direction. In a separate study a biodegradable bilayer hydrogel actuator comprising cross-linked PNIPAM and polycaprolactone (PCL) was investigated by Ionov and coworkers.[37] A patterned star-shaped bilayer actuator was fabricated by photolithography, using benzophenone derivatives as a photo-crosslinker in the UV region. For the thermosensitive layer, 1 mol% of 4-acryloylbenzophenone (ABP) was taken as the comonomer along with poly-(N-isopropylacrylamide) to synthesize the copolymer poly(NIPAM-ABP). A poly(NIPAM-ABP) layer was deposited on silicon wafer by dipcoating and on top of it a PCL layer containing 6 mol% of 4-hydroxybenzophenone (both layers were 4 mm in thickness). Then, patterned bilayer films were formed by irradiating with UV light ($\lambda = 254$ nm) through a mask. The bilayer hydrogel was able to fold and unfold in one direction on account of reversible swelling and deswelling of the PNIPAM layer in response to external temperature changes. It is worth emphasizing that the hydrophobic PCL layer used here restricted the swelling of the PNIPAM layer to only one direction. In a recent study, Aida and coworkers reported an impressive PNIPAM-based layered hydrogel actuator (PNIPA/titanate(IV) nanosheet (TiNS$_∥$)) with cofacially oriented unilamellar electrolyte TiNSs embedded in its matrix. This actuator demonstrated thermally stimulated anisotropic lengthening and shortening through internal conversion of isotropic energy into a directional mechanical motion.[38] To fabricate the hydrogel actuator, an aqueous solution of monomer NIPAM (8.0 wt%), BIS (0.48 wt%) as cross-linker, along with a colloidal dispersion of semiconducting TiNSs (1.6 wt%) was placed in a superconducting 10 T magnetic field and irradiated by UV light ($\lambda \approx 260$ nm). Upon UV irradiation TiNSs generate hydroxyl radicals that trigger in situ radical polymerization of NIPAM and BIS, forming a self-standing hydrogel network with TiNSs embedded into the matrix. In the presence of a magnetic field, the TiNSs align orthogonally to the magnetic flux and cofacial to each other so that electrostatic repulsion arises between them. At temperatures higher than the LCST, a switch in the electrostatic permittivity of the hydrogel due to loss of water molecules from the matrix results in increased electrostatic repulsion between TiNSs, which further leads to macroscopic elongation of the hydrogel. Conversely, on cooling hydration of the hydrogel leads to decreased repulsion between TiNSs, resulting in contraction of the hydrogel (**Figure 1**). Importantly, even in the absence of water, the hydrogel film lengthens and shortens, as a result of the increase and decrease in cofacial TiNS distance on heating and cooling, respectively (Figure 1A). To investigate the thermal deformation of the PNIPAM/TiNS$_∥$ hydrogel, the sample was prepared in such a way that the TiNS plane was orthogonal to the longer axis of the capillary and dipped alternately in two water baths held at two different temperatures, i.e., −15 and 50 °C. When heated at 50 °C, the hydrogel responded instantaneously by expanding along the longer axis, increasing the length by 170% (in 1 s). On reducing the temperature, the hydrogel quickly regained its original length. Quite contrary to the conventional PNIPAM-based hydrogels, which shrink and expand isotropically on heating and cooling, respectively, the anisotropic deformation rate observed for the PNIPAM/TiNS$_∥$ hydrogel was ≈70% s^{-1}. The associated contraction in the thickness of the hydrogel (i.e., ≈18% along the direction orthogonal to the long axis) on heating indicates that the hydrogel remains unchanged in volume. It is worth mentioning that in this example the anisotropic deformation did not occur when the TiNSs were randomly distributed in the hydrogel matrix (Figure 1B). Therefore, the orientation of the negatively charged TiNSs and the LCST transition of the PNIPAM hydrogel matrix is integral to thermally assisted shape transformation. Simultaneous LCST transition was found to be also essential for the actuation, which was proven by preparing an analogous hydrogel film taking N,N-dimethylacrylamide (DMA) as the monomer instead of NIPAM. Poly(N,N-dimethylacrylamide) (PDMA) does not undergo LCST transition, and consequently the PDMA film did not show any shape deformation on heating. In addition, because the actuation can be realized without uptake and release of water, this system can be used in a nonaqueous medium, ionic liquids, and open-air environment. Subsequently, to demonstrate unidirectional walking, an L-shaped symmetrical bipedal object was designed and subjected to alternating cycles of heating and cooling (Figure 1C). On heating, the back foot of this object elongates, causing the object to move forward, and by doing so, the centroid of the object is shifted toward the front side, whereas on cooling, the object shortens its elongated back foot and is drawn backward, causing
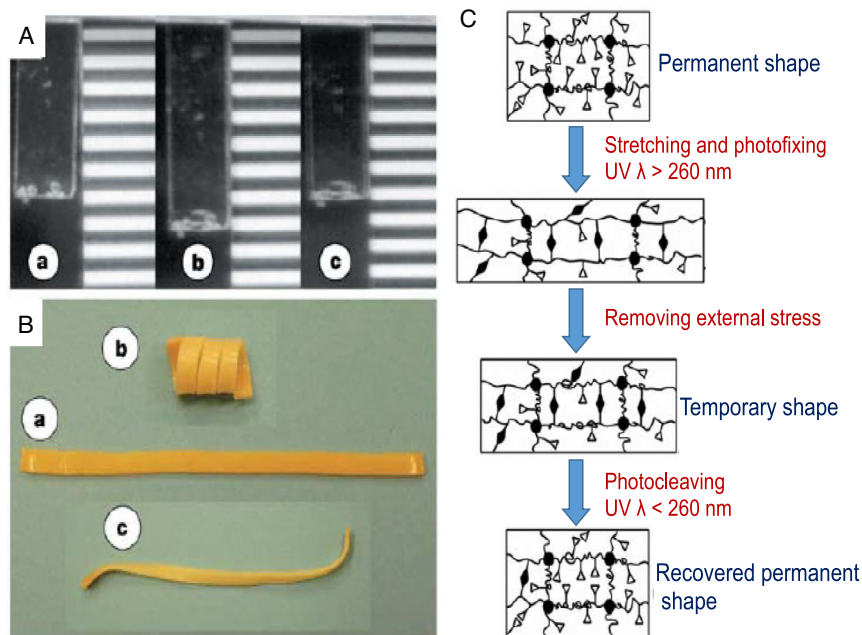
**ADVANCED
SCIENCE NEWS**
www.advancedsciencenews.com

**ADVANCED
INTELLIGENT
SYSTEMS**
Open Access
www.advintellsyst.com

Figure 1. A) Schematic representation of thermoreversible actuation of PNIPAM/TiNS$_{||}$ hydrogel. B) Schematic illustration and photographs of thermoresponsive behavior of PNIPAM/TiNS$_{||}$ (left) and PNIPAM/TiNS$_{random}$ (right). C) Unidirectional "walking" motion of L-shaped PNIPAM/ TiNS$_{||}$ hydrogel actuator. Adapted with permission.[38] Copyright 2015, Macmillan Publishers Limited.

an overall displacement of the object. Although thermally stimulated shape transformation has been widely studied for use as actuators, one major limitation is the relatively slow response rate and uncontrolled actuation, which restricts their practical use.[39]

2.2. Photoresponsive Actuators

Photoresponsive SMPs promote actuating behavior at ambient temperatures by means of remote activation. High spatial resolution and controllable intensity of the light source make them very attractive candidates for soft robotics. Photoresponsiveness can be introduced in the polymers by incorporating photosensitive chromophores, such as azobenzene (*cis-to-trans* photoisomerization), cinnamic groups (photoreversible [2 + 2] cycloaddition reactions), or spiropyran (ring opening and closing photoisomerization), into the side or main chains of the polymers. Within this context, liquid crystalline elastomers containing azobenzene functionality in the side chain belong to a new type of photochemically driven actuator that utilizes nematic (N)-to-isotropic (I) phase transition for motion.[40] The light-driven *trans-to-cis* isomerization of the azobenzene groups induced a conformational change in the polymer backbone, leading to N-to-I phase transition, expressed macroscopically as 1D contraction of the polymer. Several methacrylate elastomers were prepared varying the azobenzene-based monomer feed ratio. The elastomers were prepared by irradiating the precursor mixture taken in a liquid crystal cell with red light ($\lambda > 600$ nm). As the azo chromophore absorbs light strongly up to 550–600 nm, a photoinitiator that can be activated at wavelength greater than 600 nm was needed.

For that purpose, 1,3,3,1′,3′,3′-hexamethyl-11-chloro-10,12-propylene-tricarbocyanine triphenylbutyl borate (CBC), a photoinitiator in the near-infrared (NIR) region, was used. In this case, films with a thickness around 20 μm and lateral dimensions of 1.5 cm × 3 cm were prepared by photopolymerization. To investigate the photoresponsive behavior, the films were maintained at a temperature of 70 °C, which is well below their thermal N–I phase transition and irradiated with UV irradiation ($\lambda = 365$ nm). The extent of contraction of the elastomer films was found to be near about 12–18%, generally increasing with the intensity of the light used. A slow but complete reversal of the contraction in the film due to *cis-to-trans*-photoisomerization of the azobenzene group was observed when the UV source was switched off. Although the UV-triggered contraction of the elastomer films was very fast (time taken was less than 1 min), the thermal back reaction was comparatively slow (0.5–1 h). However, the *cis-to-trans* thermal relaxation time can be decreased by modifying the core of the azobenzene or adding a substituent to the azobenzene moiety in liquid crystalline polymers. The resulting polymer films, when attached to a substrate, exhibit continuous, directional, and macroscopic waves under illumination and are attractive candidates as miniaturized systems for transport. From a mechanistic perspective, the splay-aligned configurations of the liquid crystal network, with homeotropic alignment at one surface and planar alignment at the other, resulted in the directional propagation of waves due to the expansion and shrinkage behavior of the planar and homeotropic sides.[41] In an entirely different approach, Lendlein et al. designed a series of polymers bearing cinnamic groups and investigated the shape memory properties. For this, two series of grafted polymers and interpenetrating networks

ADVANCED
SCIENCE NEWS
www.advancedsciencenews.com

ADVANCED
INTELLIGENT
SYSTEMS
Open Access

www.advintellsyst.com

Figure 2. Shape memory effect of A) grafted polymer film: a) permanent shape, b) temporary shape, c) recovered permanent shape; B) IPN polymer film: a) permanent shape, b) temporary shape, c) recovered shape. C) Illustration of shape memory effect in grafted polymer film. Adapted with permission.[42] Copyright 2005, Nature Publishing Group.

(IPNs) were prepared that can be deformed into predetermined shapes such as elongated film, arches, or spirals through UV light irradiation (**Figure** 2A,B).[42] The polymers regained their original shape when irradiated with a different wavelength of UV light, at ambient temperatures. Importantly, these new shapes were found to be stable for a long time period and at high temperature. Specifically, the molecular switches used to study the shape memory effect are photosensitive cinnamic acid (CA) and cinnamylidene acetic acid (CAA). When exposed to alternating wavelengths (here: $\lambda > 260 \, \text{nm}$ or $\lambda < 260 \, \text{nm}$), photoreversible $[2 + 2]$ a cycloaddition reaction takes place between the alkene functionalities in CA or CAA, forming a temporary crosslinking point. On stretching the photoresponsive polymer film to 20% elongation by external stress, coiled segments in the amorphous domains of polymer chains between two net points were uncurled and elongated. Then, new photoresponsive cross-links were formed between the expanded regions of the chains by irradiating with UV light of $\lambda > 260 \, \text{nm}$, forming an elongated temporary shape. The elongation rate was maintained at $10 \, \text{mm} \, \text{min}^{-1}$ during the measurement, and the original permanent shape could be recovered by cleaving the photoresponsive cross-links with UV light of $\lambda < 260 \, \text{nm}$ (Figure 2C). The strain-fixity rate R_f (N) as well as the strain-recovery rate R_r (N) of the Nth cycle was calculated using the following equations

$$R_f(N) = \varepsilon_u(N)/\varepsilon_{max} \tag{1}$$

$$R_r(N) = (\varepsilon_{max} - \varepsilon_p)/\varepsilon_{max} \tag{2}$$

where ε_{max} is the initial elongation of the polymer film under constant stress, ε_u is the elongation in the temporary shape,

and ε_p is the remaining elongation after recovery of permanent shape. The R_f defines the ability of molecular switches to fix the mechanical deformation of temporary shape, applied during the photo-crosslinking process and R_r defines the ability of the material to regain its original shape. Other temporary shapes can also be produced by selectively irradiating one of the surfaces of the polymer film in a stretched state (100% elongation). While the irradiated surface deforms to a certain extent, the opposite surface maintains its elasticity. The difference in elasticity of the two opposite surfaces results in an arch or corkscrew spiral shape after the external stress has been removed. The results showed that IPN polymers showed an R_f (%) of 20–33% and an R_r (%) of more than 88%, while graft polymers showed R_f (%) of 11–38% and an R_r (%) of more than 98%. To rule out the possibility of photothermal conversion effect, the temperature of the polymer films was measured during the process by placing a digital thermocouple in the films. The fluctuation in the temperature was found to be small ($\pm 0.18 \, ^\circ\text{C}$) during the irradiation period, which indicates that thermal energy does not stimulate shape deformations in the polymer films. This is an important control measurement that should be routinely done to describe accurately the underlying mechanism of polymer actuation.

Following a similar approach, Sun and coworkers designed and synthesized a biocompatible and biodegradable multiblock polyesterurethane-based shape memory polymer, containing photoresponsive cinnamamide groups in the side chain (**Figure 3**).[43] Multiblock polyesterurethanes composed of PCL and the photoresponsive cinnamamide groups as biodegradable soft segments and poly(L,L-lactide) (PLLA) as hard segments were synthesized via a SnOct$_2$-catalyzed two-step polyaddition reaction
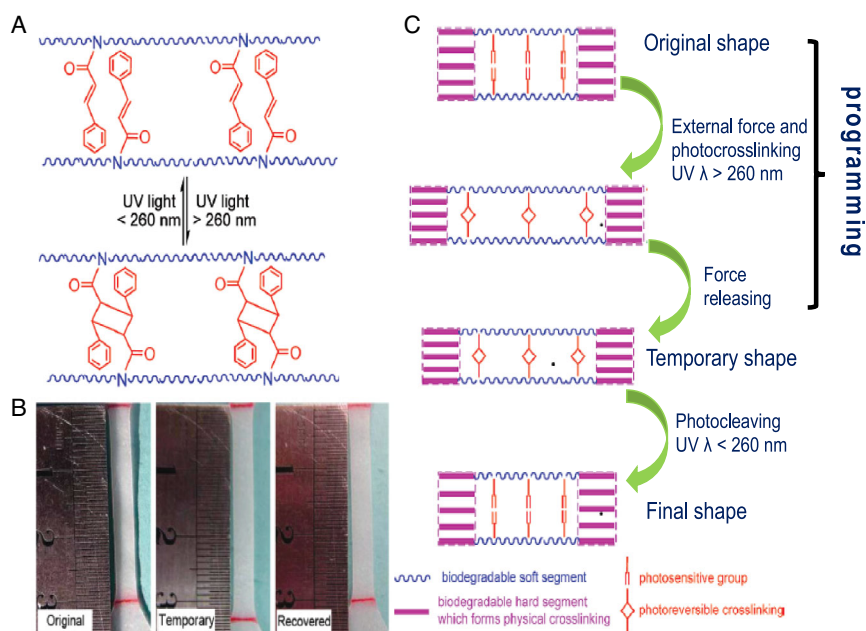
Figure 3. A) Light-induced [2 + 2] cycloaddition reaction involving cinnamamide groups in the polymer side chain. B) Digital photographs showing macroscopic shape memory behavior triggered by UV irradiation. C) Schematic of shape memory effect in photoresponsive multiblock polyesterurethane. Adapted with permission.[43] Copyright 2011, American Chemical Society.

of biodegradable polyester diols and a photoresponsive monomer with hexamethylene diimide. Here, the hard phase acts as the physical cross-link and enhances the mechanical strength of the copolymer, while the chain flexibility and low transition temperature of the soft phase endow the copolymer with flexibility. The multiblock copolymers showed very high elongation (230–530%), satisfactory tensile modulus (20–230 MPa), and strength (10–21 MPa). The elongation increased with increasing content of soft PCL segments. The photoinduced shape memory property was evaluated by calculating the R_f and R_r using Equation (1) and (2). The polymers showed R_f in the range 32–55% and a very high R_r (>95%). In general, the shape memory behavior of the polymer depends on the polymer composition. R_f increased with increasing content of cinnamamide in polymers and R_r increased with increased content of PLLA. In vitro hydrolytic degradation of four copolymer samples in phosphate-buffered saline at 37 °C showed that the polymers lost 12–25% weight in 32 weeks, preliminarily indicating hydrolytic degradability. The slow degradation rates were attributed to the slow degradation of PCL and PLLA homopolymer segments.

Photoinduced stress generated in a stretched azobenzene containing a liquid crystalline elastomer (azobenzene-containing liquid crystalline elastomer (ALCE)) film under UV light illumination can be amplified by conserving the mechanical strain energy in the polymer.[44] The prestored strain energy, along with the photoisomerization of azobenzene mesogens, can be used to generate a mechanical deformation or actuating motion by exposure to UV light. Results from isostrain measurements revealed that the photoinduced stress in ALCEs was much higher than that generally found in ALCEs and it increased with increase in applied strain. The magnitude of the photoinduced stress

controlled the speed of the light-driven actuator, while the direction of the motion, i.e., motion toward or away from the light, was controlled by the 3D architecture of the actuator. Results showed that the actuator with higher prestored strain energy moved at a faster speed than the actuator with lower prestored strain energy under the same intensity of UV light. As the stress generated in ALCEs also depends on the intensity of the UV light used at a given strain (higher intensity results in larger stress generation), the speed of an actuator can be adjusted by changing the light intensity. The fabrication strategy of the aforementioned photoresponsive systems involves reshaping of polymers into a temporary shape by means of a mechanical force. Development of advanced biomimetic walking soft robots, which does not require reshaping or programming into a temporary shape, will widen the scope of photoreversible actuators in cargo transport, sensing, and targeted drug delivery. A P(NIPAM-co-SP-co-AA) (SP–spiropyran, AA–acrylic acid) based hydrogel walker with SP as the photosensitive moiety is a synthetic system in which walking motion can be achieved by reversible shrinkage and expansion of the gel network using repeated "on/off" white light irradiation as trigger.[45] The molecular mechanism involves protonation of photoresponsive SP in an acidic environment generating more hydrophilic protonated merocyanine species (MC-H$^+$), which absorbs water from the surrounding medium, thereby leading to expansion of the hydrogel. Upon exposure to white light ($\lambda_{max} = 422$ nm), MC-H$^+$ releases a proton prompting it to isomerize back to the more hydrophobic SP form leading to expulsion of water and contraction of the gel (**Figure 4**A). Very elegantly, arc-shaped hydrogel walkers were prepared by photolithography, using a cell consisting of a poly(methyl methacrylate) (PMMA) mask, glass slide, and glass cover slide separated by a 500 µm high PMMA/pressure-sensitive adhesive.

2000214 (6 of 19)
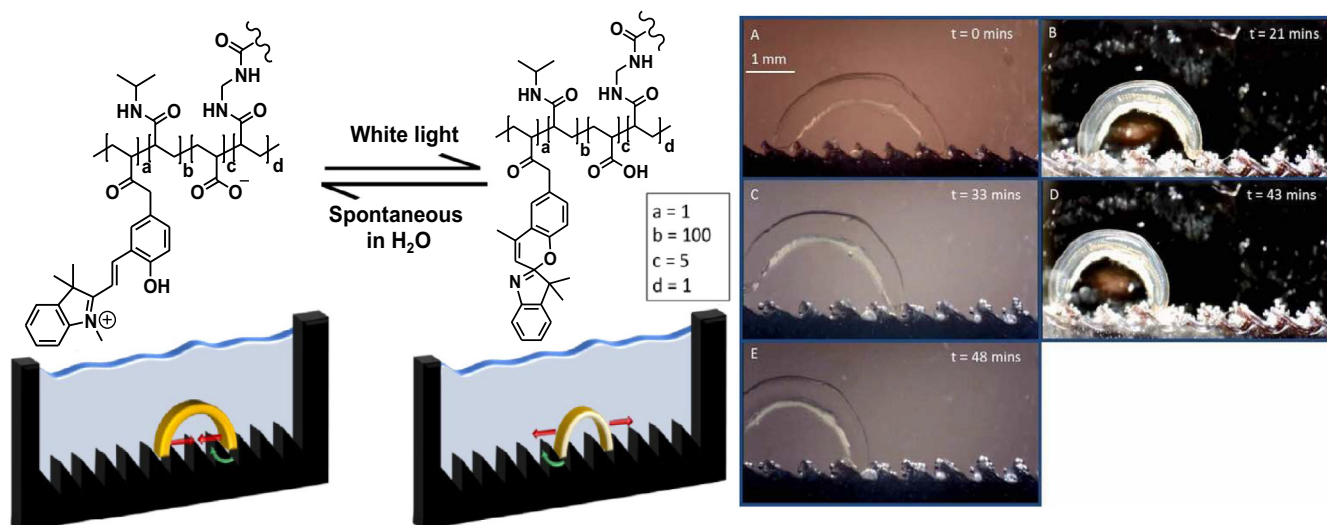
Figure 4. (Left) Schematic of expansion/contraction of p(NIPAM-*co*-SP-*co*-AA) hydrogel walkers under different light irradiation. (Right) Photographs showing light-triggered "walking" motion of the gel. A) Light irradiation is initiated. B–E) Gradual reduction of interleg distance resulting in the trailing leg (right) being "dragged" over the ratchet step. Adapted with permission.[45] Copyright 2017, Elsevier B.V.

The PMMA mask had an array of walkers, each of which was 1.44 mm high and 0.56 mm wide with 2.81 mm (outer) distance between the legs. A monomer solution taken in the cell was photopolymerized through the mask by white light with intensity 310–320 kLux. The alternate expansion/contraction of the gel can be utilized to mimic 1D "walking" on a ratcheted surface. The "walking" behavior of the hydrogels was realized by placing a single walker on to one of the ratcheted channels (45 mm × 1 mm × 12 mm) filled with deionized water (Figure 4B-D). The individual ratchets were 0.5 mm high and had 7 mm distance between two consecutive ratchets. The white light source used to monitor the walking motion had an intensity of ≈305 kLux. Importantly, the polymerization time and cross-linking density affected the motion. Specifically, the walker with higher polymerization time was found to have better reversible actuation. It should be considered that the actuation behavior (swelling, contraction) in hydrogels is a diffusion-controlled process and the actuation kinetics can be improved by increasing the hydrogel pore density. To achieve maximum actuation by the hydrogels, it is necessary to have ratchets of optimal dimension. In this sense, to design ratchets of appropriate dimension accurate measurement of the distance between the legs before and after actuation is required.[39]

A photoresponsive bilayer swimmer that can exhibit controlled, directional motion at the liquid/air interface can be fabricated using an azobenzene-containing liquid crystalline polymer network and the polyimide Kapton. The bilayered film exhibits quick bending toward the Kapton side upon illumination by UV light and recovers immediately after removal of the light. In this case, self-propelling propagation of the swimmer on a liquid surface is achieved though rhythmic beating of the liquid, which is analogous to the "dolphin kick."[46] Robotic walkers can be constructed using a polyethylene (PE) film laminated with a layer of a cross-linked liquid crystalline polymer (CLCP).[47] The CLCP layer is composed of an azobenzene-containing polymer in which the azobenzene mesogens are in the smectic phase, aligned along the long axis of the film. Compared to the nematic phase, mesogens in the smectic phase show highly ordered arrangement and generate larger mechanical deformation on exposure to UV irradiation. The CLCP layer (16 μm) was attached on the PE film (50 μm) through an adhesion layer by thermal compression. Because of the different thermal expansion coefficients of the CLCP and PE layers, the CLCP-laminated portion of the film remain curled up. *Trans*-to-*cis* photoisomerization of the azobenzene functionality in the CLCP layer under UV light ($\lambda = 366$ nm) produces a contraction force along the alignment direction of mesogens, which results in extension of the laminated film. Conversely, when exposed to visible light ($\lambda > 540$ nm), the film goes back to the original bent shape because of *cis*-to-*trans* back-isomerization.

Photothermal conversion materials convert energy from visible or NIR light to thermal energy and are often used in thermally responsive hydrogel matrices to trigger volume phase transition in hydrogels. The main trigger mechanism in such materials is thermal heat generation by absorption of light in the hydrogel matrix, which in turn leads to volume shrinkage of the temperature-responsive hydrogel. A photoresponsive hydrogel actuator that can generate rapid repeatable elongation/contraction movements by means of photothermal switching of electrical permittivity of the hydrogel interior, leading to astounding earthworm-like unidirectional motion, without uptake and release of water, was reported by Aida and coworkers.[48] In terms of composition, the hydrogel contained gold nanoparticles (AuNPs) for photothermal conversion, a thermoresponsive PNIPAM network that reversibly changed the electrical permittivity of the hydrogel matrix and cofacially oriented negatively charged TiNSs for anisotropic electrostatic repulsion–induced elongation and contraction (**Figure 5**A,B). The crawling motion of the TiNS/AuNP hydrogel was triggered by irradiating the gel with a 445 nm laser spotlight (5.0 mm × 1.8 mm
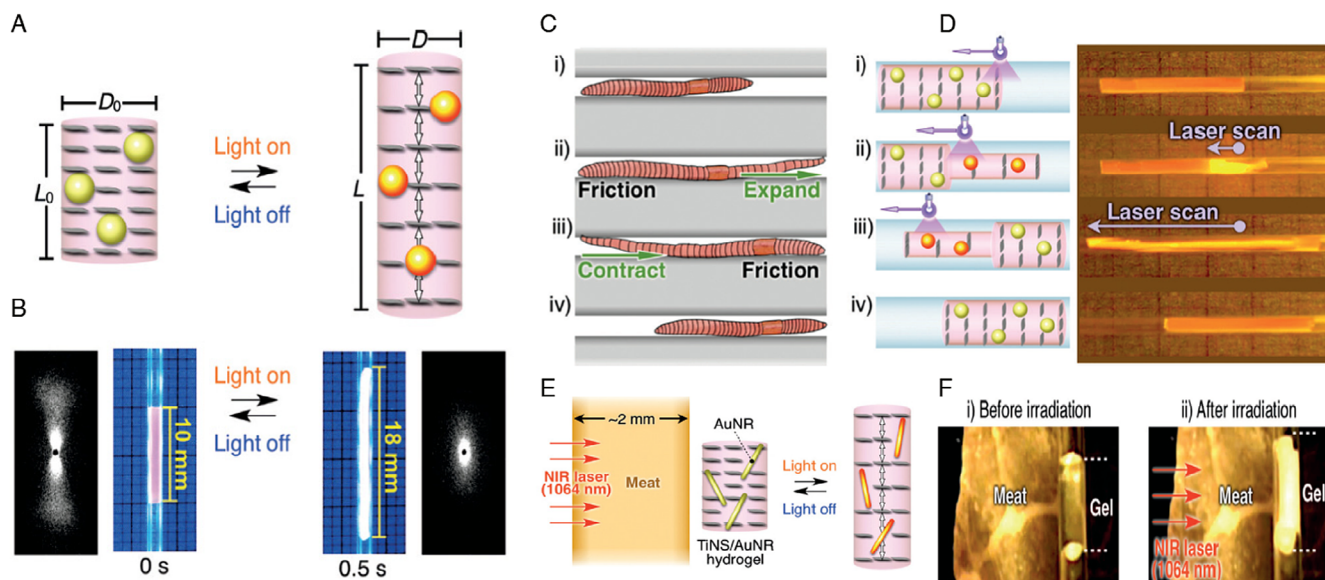
Figure 5. A) Schematic illustration of light triggered actuation of TiNS/AuNP hydrogel. B) Digital photographs and 2D small-angle X-ray scattering (2D SAXS) images of a hydrogel cylinder held in a capillary. C) Illustration of the peristaltic crawling of an earthworm. D) Optical images of a cylindrically processed TiNS/AuNP hydrogel taken through a laser safety filter. E) Schematic of NIR-triggered actuation of TiNS/AuNR hydrogel through a ≈2 mm thick piece of meat. F) Optical images of TiNS/AuNR hydrogel taken through a laser safety filter. Adapted with permission.[48] Copyright 2018, John Wiley & Sons.

rectangular spot, 5.6 W cm^{-2}). When the hydrogel was irradiated at one end, the region became thinner, decreasing the friction with the capillary wall, and lengthened by 180% in <0.5 s. The hydrogel regained its original length within 6 s on turning off the laser light. On moving the irradiation spot toward the other end at a velocity of 3.4 mm s^{-1}, spatiotemporal expansion/thinning followed by shape recovery occurred sequentially along the laser scanning direction, moving the hydrogel toward the direction opposite to the scanning direction (Figure 5D). Remarkably, a displacement of 7 mm was achieved by one single laser scan. As gold nanorods (AuNRs) are known to convert NIR light into thermal energy, an NIR-responsive hydrogel was prepared by introducing AuNRs into the hydrogel matrix instead of AuNPs (TiNS/AuNR hydrogel). The temperature of the hydrogel could be raised to 67 °C within 30 s of irradiation with a 1064 nm laser light (12 W cm^{-2} power density). A cylindrical TiNS/AuNR hydrogel (1.2 mm diameter, 5.0 mm length) lengthened by 130% within 3 s in the direction orthogonal to the TiNS plane. Further, the hydrogel cylinder when irradiated with the NIR laser light through a 2 mm thick piece of meat deformed within 6 s and can be used in biomedical applications (Figure 5E,F).[39]

Graphene is also known as a promising photoconversion material with excellent solar energy–harvesting efficiency, efficient transformation of photoenergy into thermal energy, ultrathin dimensions, high transparency, excellent mechanical strength, and adjustable thermal conductivity. The extended 2D planar structure of large-area graphene consisting of conjugated carbon atoms allows excellent absorption of IR light and the one-atom height of the 2D material imparts high visible-light transparency. A bilayer, transparent soft actuator composed of chitosan and PE can be constructed by introducing large-area graphene that utilizes IR light as the driving energy to trigger actuating motion.[49] To construct the actuator strip, a PE film affixed on a glass substrate was taken and the film surface was made hydrophilic by treatment with a mixture of H$_2$SO$_4$ (2 mL), HNO$_3$ (2 mL), and CrO$_3$ (10 mg). The modified PE film was homogeneously coated with a mixture of large-area graphene/chitosan to form a transparent thin large-area graphene–chitosan/PE film. Actuation in the film was found to be driven by the high stress generated at the interface area of PE/chitosan. At room temperature in absence of IR light irradiation, the film remains in an initial contracted state, which transforms into a flat, stretched state on irradiation with IR light. When the actuator strip stretches in the presence of IR light, the head edge slides along forward direction on the substrate, while mechanical symmetry restrains the rear edge from sliding backward. As soon as the IR light is turned off, contraction of the strip begins, dragging the rear edge forward and at the same time preventing the head edge from sliding backward. Alternate on–off switching of the IR light triggers repeatable contraction and stretching of the film, resulting in 'walking' of the strip in the forward direction. Polydopamine (PDA), a new type of organic photothermal agent, shows excellent photostability, strong absorption, and negligible resonance light scattering in the NIR region, which indicates high photothermal conversion efficiency. Moreover, it shows good compatibility with polymeric systems, such as liquid crystal elastomers (LCEs).[50] Interestingly, the photothermal effect of PDA in a robotic swimmer composed of a PDA-coated LCE film enables the swimmer to perform "swimming strokes" through reversible bending/unbending motions and to swim near the water–air interface.[51]

2.3. Electric Field–Responsive Actuators

Electroresponsive hydrogel actuators operate by converting electrical energy from the power source into mechanical energy, i.e., shape distortion of the hydrogel. Generally, polyelectrolytes having ionizable groups in the backbone or in the side chains of the polymer networks are responsive to electric stimuli. Essentially, when exposed to an electric field the free ions in the medium undergo directional migration (i.e., cations to a cathode and anions to an anode) and rearrangement of the fixed charges occurs at the interface of the hydrogel and swelling medium. In case of nonuniform distribution of the ion concentration inside and outside the gel, an osmotic pressure difference is generated that leads to swelling, deswelling, and bending of the hydrogel, transforming electrical energy into mechanical motion. Calvert and coworkers prepared an electrically driven hydrogel actuator consisting of layers of cross-linked polyacrylamide (PAAm) deposited on layers of PAA, which undergoes uniaxial contraction/expansion motion on alternating acid/base treatment without expulsion of water from the hydrogel.[52] The water gets internally transferred from polyacrylate (as it neutralizes to PAA in the acidic solution) to PAAm. The PAA layer shrinks on expelling water from its hydrogel layers, with subsequent deformation in PAAm layers due to uptake of the expelled water from the PAA layer. The deformation in the system depends upon the degree of dissociation of the PAA layer and the ionic strength of the medium. Electrolysis of water due to flow of current creates a pH gradient that drives the shape change. The hydrogel was made up of six gel layers—two of PAA and four of PAAm—and the electric field–driven actuation was performed by placing the layered hydrogel, previously swollen in a 0.1 M phthalate buffer at pH 5, between carbon foil electrodes at 3 V on a dry plate. The results showed that contraction along two horizontal axes due to water expulsion from the PAA layer was accompanied by a thickness change along the vertical direction ($\approx$10% in 1 min at 3 V) due to water uptake by PAAm layers. The thickness change was measured by recording the deflection of a laser reflected off the horizontal top surface of the stack on a vertical scale. The water uptake capacity of the PAAm could be improved by decreasing the cross-link density of the PAAm to about half that of the PAA. Overall, the study demonstrates that stacked layers of PAA/PAAm hydrogels show linear contraction, instead of bending, in response to an applied electric field. In another study, a gel system in which complex locomotion mimicking a snake-like trail could be realized and precisely controlled over a long path range by nonionic polymer gels in response to an electric field was developed and investigated. The polymer gel system composed of a poly(vinyl alcohol)/dimethyl sulfoxide (PVA/DMSO) gel could exhibit such movement in air when operated by a direct current.[53] To prepare the polymer gel, PVA was dissolved in a boiling mixture of DMSO:water (72 wt%:18 wt%) solution and poured into a glass mask. A physically cross-linked gel was formed when the solution in the glass mask was cooled and maintained at −20 °C for 12 h. Subsequently, the formed polymer gel was immersed in glutaraldehyde solution (0.07 wt%) for 8 h, maintaining solution temperature at 5 °C. Thereafter, the gel was chemically cross-linked by heating at 30 °C for 1 h, and the solution pH was adjusted to 2–3 with HCl solution prior to heating. Finally, the block was washed with methanol/DMSO solution and the gel swollen in DMSO. In this example, the experimental setup to study the locomotion of the polymer gel consisted of two thin gold electrodes (15.0 mm × 12.0 mm × 0.5 mm) fixed on a glass substrate with a 100 μm thick insulating adhesive film. A DMSO liquid line (2.0 mm wide and 10 μm thick) cast on the glass substrate connected the two electrodes. A 6.0 mm long cylindrical PVA/DMSO gel rod with a radius of 1.5 mm and swelling degree 98.7 wt% was made to crawl quickly from anode to cathode along a designed path under an applied DC electric field (**Figure 6**). The experiments were performed in air under ambient conditions of $T = 288$ K and relative humidity (RH) of $H = 23.6\%$. The microcurrent generated between the electrodes due to the applied voltage was measured using an ampere meter. The obtained results indicated that the average crawling speed can reach up to $v = 14.4$ mm s^{-1} on a linear path and $v = 5$ mm s^{-1} on a curvilinear path under the electric field of $E = 400$ V mm^{-1}.
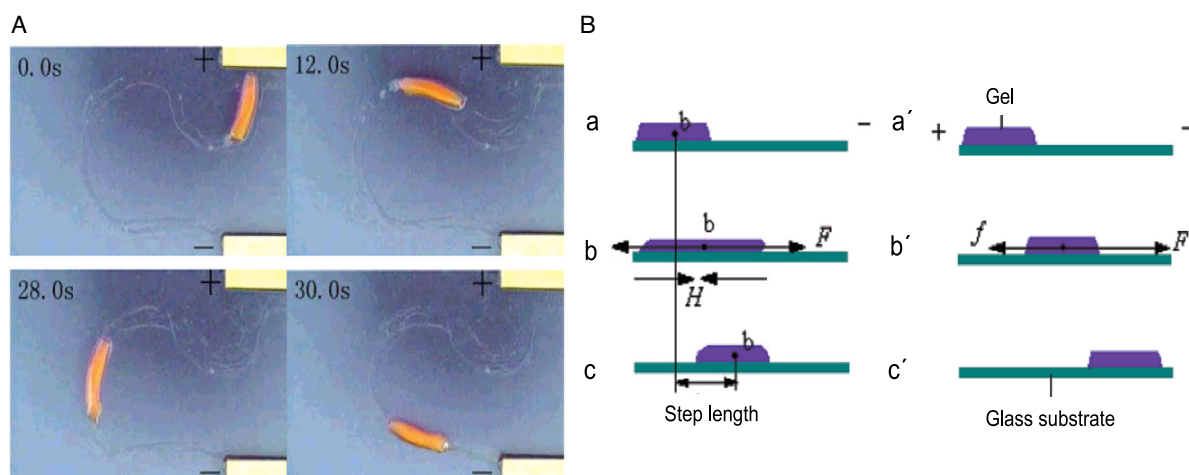

Figure 6. A) Digital photograph showing the trail of a hydrogel in an electric field (DC). B) Schematic of the gel showing snail-like walk under the applied electric field. Adapted with permission.[53] Copyright 2017, American Chemical Society.

ADVANCED
SCIENCE NEWS
www.advancedsciencenews.com

ADVANCED
INTELLIGENT
SYSTEMS
Open Access
www.advintellsyst.com

However, in this example a minimum threshold of the applied electric field is needed to get the gel moving along the designed path. This minimum applied electric field has been defined as the critical driving threshold (E_{cg}). An important aspect of this system is that controlled motion arises from the flow of DMSO inside and outside the polymer network. Under the DC electric field, charges move in DMSO from the anode to the cathode under electrostatic forces and trigger the flow of the solvent inside and outside the polymer network, which has been used to generate movement. The crawling speed of the gel depends both on the strength of the applied electric field and on the swelling degree of the gel. Soft robots constructed from hydrogel materials that use electric stimuli are of significant importance as they make remote control of the strength and direction possible and provide a rapid on/off trigger.[39]

Yang and coworkers prepared an arc looper–shaped hydrogel walker composed of cross-linked polyanionic poly(2-acrylamido-2-methylpropanesulfonic acid-co-acrylamide) (poly(AMPS-co-AAm)) networks.[54] One-directional walking motion can be realized through reversible bending and stretching of the hydrogel on a rough surface when exposed to repeated "on/off" electrical fields in electrolyte solution, and can be used to transport very heavy cargo (**Figure 7**A). The authors synthesized the looper-shaped hydrogel walkers by free radical polymerization in a mold setup with a quartz glass plate, a Teflon plate spacer (0.3 mm thick), and a Teflon plate held together by clamps. Polymerization was conducted in the mold by irradiating with UV light for 20 min from the quartz glass side. After purification of the hydrogel, poly(AMPS-co-AAm) was cut into uniform strips of hydrogel having dimensions 10.0 mm × 2.0 mm × 0.5 mm for further investigation. The gradual decrease in UV light strength along the irradiation distance imparts a gradient in distribution of cross-links in the hydrogel network along the spacer height. Due to the anisotropy in the polymer network, the hydrogel strips bend to the more densely cross-linked side in water, resulting in arc-shaped walkers containing two legs. The AMPS imparts

electroresponsiveness on account of its strongly ionizable sulfonate group, while the AAm is incorporated to improve the mechanical strength of the fragile poly(2-acrylamido-2-methylpropanesulfonic acid) (PAMPS) hydrogel. The electric field–induced walking motion was studied by placing the hydrogel walker on a resin plate with a ratchet surface, immersing the whole setup in 0.01 mol L^{-1} NaCl solution. The ratchet plate was horizontally placed between two carbon electrodes and an electric voltage (25 V) was applied. To generate the reversible bending/stretching movements, the hydrogel walker was exposed to an alternating electric field, turning on for 10 s and turning off for the next 15 s (Figure 7B). To determine the effect of the ratchet topography on the walking motion, plates with different step sizes ($m \times n$) of 0.4 mm × 0.2 mm, 0.8 mm × 0.2 mm, 0.8 mm × 0.4 mm, and 1.2 mm × 0.2 mm were used. As walking motion was observed on the ratchet plate with $m \times n = 0.8$ mm × 0.2 mm, such a plate was used to investigate cargo transportation. The effect of the cargo weight on the walking efficiency (walking velocity, displacement achieved) of the poly(AMPS-co-AAm) hydrogel walkers was investigated by loading the hydrogel walkers with different weights of cargo, 25, 50, 75, 100, and 125m_0 (Figure 7C). The results showed that the walking distance decreased from 13.44 to 7.16 mm after and walking velocity decreased from 8 to 4.2 mm min^{-1} with increasing the cargo weight. This is because an increase in cargo weight raises the pressure of the loaded hydrogel on the ratchet, which in turn increases the resistance caused by the surface friction against the movement and also restricts the bending of the hydrogel. The bending/stretching deformations of the hydrogel walkers and, therefore, the unidirectional "walking" motion can be tuned by regulating the applied voltage.

It is also possible to construct hydrogel walkers that can walk on flat surfaces and do not have to rely on ratchet surfaces for locomotion. Such a hydrogel walker was fabricated by Velev and coworkers and comprised cationic gel legs made up of copolymer networks of acrylamide (AAm)/sodium acrylate
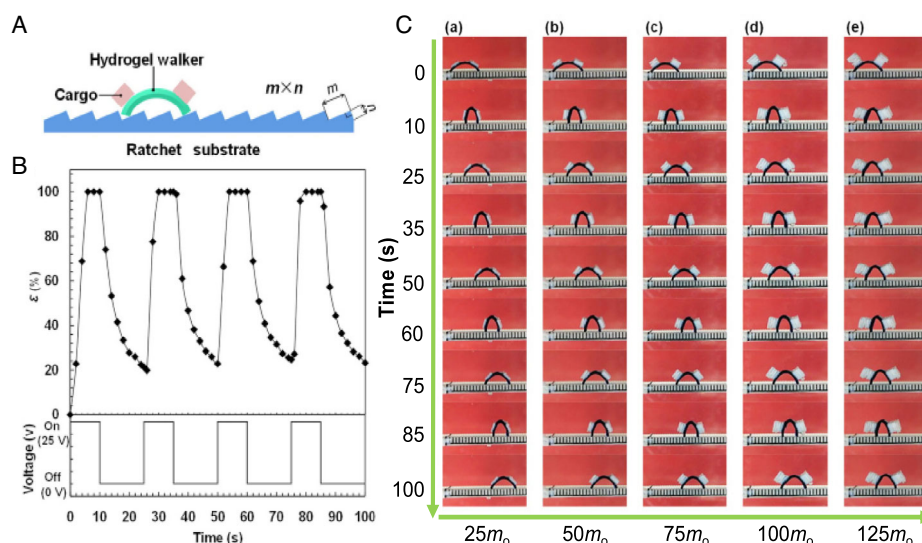
Figure 7. A) Schematic illustration of "walking" motion of a cargo-loaded hydrogel walker on a ratchet surface. B) Electric field–triggered reversible bending/stretching of the hydrogel (ε: degree of bending behavior of the hydrogel walker). C) Digital photographs showing unidirectional walking of cargo-loaded (different weights) hydrogel walkers. Adapted with permission.[54] Copyright 2015, Nature Research.
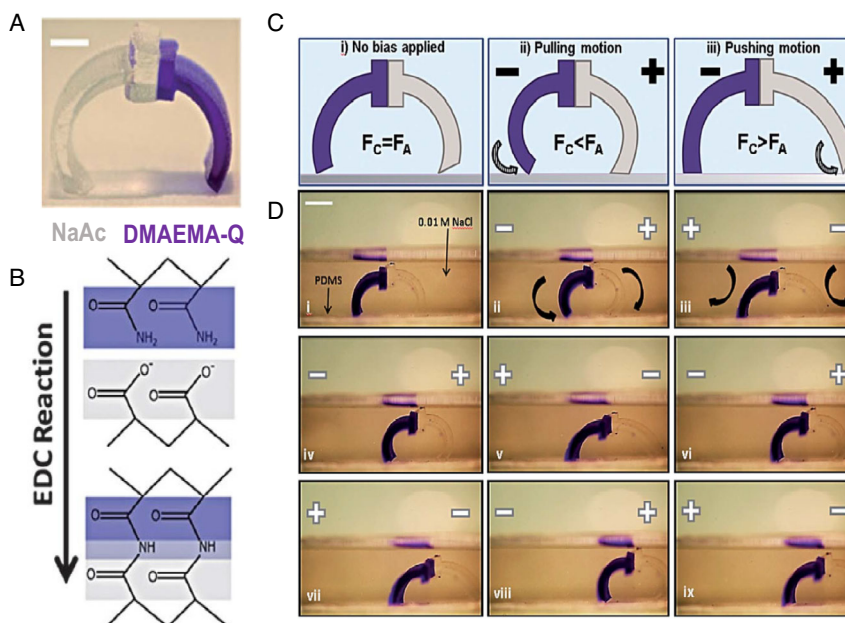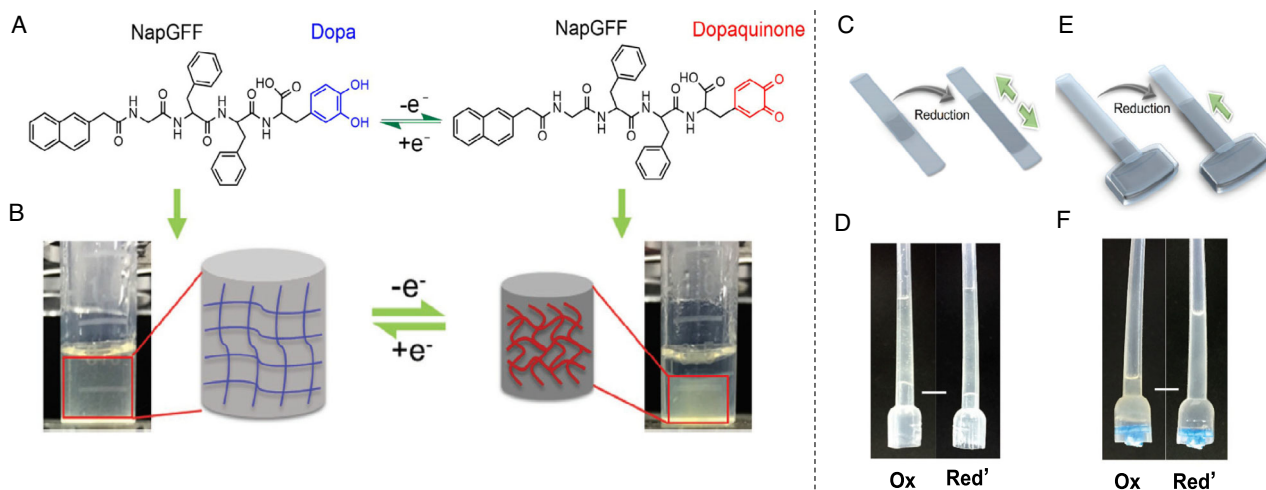
Figure 8. A) Digital photograph of a gel walker. B) Illustration of covalent "amide" bond formation between carboxylic acid and primary amine groups at the interface of two legs. C) Actuation mechanism of the gel walker based on the applied electric field (F_c and F_a are the friction forces of the cationic leg (dark blue) and anionic leg (light gray), respectively). D) Digital photographs of the gel walker under an external electric field. Adapted with permission.[55] Copyright 2015, Royal Society of Chemistry.

(NaAc) and anionic gel legs made up of AAm/quaternized dimethylaminoethyl methacrylate (DMAEMA-Q) (**Figure** 8A).[55] Cationic and anionic hydrogels were separately synthesized by free radical polymerization using BIS as the cross-linker, ammonium persulfate (APS) as the initiator, and N,N,N',N'-tetramethylethylenediamine (TEMED) as the accelerator in aqueous solution. Using a laser writer, gel appendages were cut from the bulk gels and equilibrated in 0.01 M NaCl solution. Oppositely charged leg-shaped gels were thereafter attached to each other by placing in between carbon electrodes and applying an electric field. Because of the surface charges arising from hydroxides and quarternary amine groups of the polymer, the two gel networks got attracted to each other and strong polyionic complexes were formed at the interface when an electric field ($4\,V\,cm^{-1}$) was applied for 2 min. Although polyionic complexes are stable in deionized water, they break in salt solutions due to screening of the ionic interactions by the ions in solution. Therefore, the adhesion between two hydrogels at the interface was reinforced through covalent amide bond formation between the carboxylic groups in the NaAc gel and primary amine groups in the DMAEMA-Q gel by treating with 10 mM N-(3-dimethylaminopropyl)-N'-ethylcarbodiimide hydrochloride (EDC) solution for 24 h (Figure 8B). Next, the hydrogel was equilibrated in 0.01 M NaCl solution followed by staining the cationic segment by bromophenol blue. Deformation of the legs in opposite directions when exposed to an electric field induced walking motion in the hydrogel. The experiment was conducted in 0.01 M NaCl solutions using a flat, untreated polydimethylsiloxane (PDMS) substrate as the walking surface and graphite electrodes placed 6 cm apart. The electric field ($5\,V\,cm^{-1}$) direction was controlled externally. Application of the field along the direction in which the cationic and anionic segments face the cathode and anode, respectively, caused the legs to bend inward toward each other. The anionic leg now having a larger contact area with the PDMS dragged the walker to the right. Thereafter, reversal of the field caused the anionic leg to stretch toward the cathode because of the higher friction force of the DMAEMA-Q gel leg and the cationic leg pushed the walker forward. Here, unidirectional motion was realized on a flat surface by periodic repetition of the aforementioned process (Figure 8C).

In a different study, an electroresponsive peptide-based supramolecular hydrogel containing 3,4-dihydroxyphenylalanine (DOPA) as the redox-responsive unit was prepared by Wang and coworkers.[56] DOPA can be reversibly oxidized to dopaquinone by redox or electrochemical methods (**Figure 9**A). A change in the redox states of DOPA will lead to a change in hydrophobicity of the assembled fibers, further resulting in macroscopic change in volume, elasticity, and mechanical properties of the hydrogel (Figure 9B). Unidirectional volume change by electrochemical means was achieved by constraining the diameter of the hydrogel using a PE tube. The hydrogel in the oxidized state was then reduced electrochemically, which resulted in unidirectional expansion of the hydrogel along the axis of the tube. The extent of stretching of the hydrogel can be amplified by connecting the tubing container to a sample reservoir with a much larger diameter. By capping the bottom part of the tube by a platic stopper that would prevent leakage of the hydrogel, the amplitude of elongation of the gel upon electrical reduction could be increased. The amplitude can also be modified by altering the relative diameters of the tubing and the reservoir (Figure 9C,D).[39] In this example, electrochemical switching between the redox states was conducted using an electrolyzer.

ADVANCED
SCIENCE NEWS
www.advancedsciencenews.com

ADVANCED
INTELLIGENT
SYSTEMS
Open Access
www.advintellsyst.com

Figure 9. A) Chemical structure and redox reaction of peptide-containing DOPA. B,C,E) Schematic and D,F) digital photograph of electroresponsive actuation in a DOPA-containing hydrogel. Adapted with permission.[56] Copyright 2016, John Wiley & Sons.

2.4. Magnetoresponsive Actuators

Magnetoresponsive actuators are generally fabricated by incorporating magnetic particles in the polymer network, unlike other actuators where the stimuli responsiveness is an intrinsic characteristic of the polymeric material. An external magnetic field is used to precisely and remotely control the movements and the motion is feasible in any magnetically transparent media. This makes magnetoresponsive actuators particularly useful for biomedical applications where physical contact with the actuator is not always possible. By varying the loading densities of the magnetic particles, properties of magnetoresponsive actuators can be fine-tuned. Kwon and coworkers prepared a new magnetic polymeric nanocomposite material system composed of a photocurable resin monomer and superparamagnetic colloidal nanocrystal clusters (CNCs) through an in situ fabrication process that enables programming of magnetic anisotropy in the actuator microstructure during the manufacturing process.[57] Fundamentally, the self-assembling behavior of superparamagnetic nanoparticles was combined with a spatially regulated photopatterning process to fabricate the polymeric actuator. Poly(ethylene glycol) diacrylate (PEGDA) along with 10 wt% of 2,2-dimethoxy-2-phenylacetophenone (DMPA) as photoinitiator was taken as the photocurable resin. Superparamagnetic CNCs were dispersed in the photocurable resin for the microstructure programming on nanocomposite material. CNCs consist of multiple single-domain Fe_3O_4 nanocrystals capped with SiO_2. In the absence of a magnetic field, the nanoparticles are randomly oriented in a photocurable resin but align themselves along the magnetic lines of forces forming chain-like nanostructures in a homogeneous magnetic field. The nanostructure formation minimizes the magnetic dipole interaction energy. Changing the magnetic field direction reorients the magnetic dipoles along the external field direction. Polymeric microactuators were fabricated by photopolymerization of the resin using an optofluidic maskless lithography system. The nanoparticle assembly was fine-tuned by regulating the magnetic field

direction such that all parts of the actuator moved in different directions under a homogeneous magnetic field and each of the self-assembled state was fixed by photopolymerization (**Figure 10**A). The polymeric microactuator consists of two heads, two bodies, and three joints. Each part has a different magnetic easy axis so that each part rotates in a different direction and angle in response to a homogeneous magnetic field. The two inner bodies have their magnetic easy axes parallel, while the two outer heads have their magnetic easy axes along the vertical direction with respect to the substrate, and the ladder-like joints prevent any unnecessary twisting. The arching motion of the microrobot, when an external magnetic field is applied in a vertical direction to the substrate, gets translated into a net forward displacement taking advantage of the frictional force between a head and the substrate. Thus, forward crawling motion of the polymeric microrobot can be realized by carefully regulating the magnetic field direction (Figure 10B–D). Alternatively, the periodic magnetization profile along the body of a soft robot, made of a hard magnetic neodymium–iron–boron (NdFeB) microparticle embedded silicone elastomer, can be controlled by a time-varying magnetic field and used to generate multimodal locomotion.[58]

2.5. Humidity-Responsive Actuators

In addition to the stimuli-responsive materials discussed in the previous sections, actuators that can sense and respond to minute fluctuations in humidity have also been developed. These actuators rely on uptake and release of a minute amount of water from the atmosphere for the actuating motion. Lee and coworkers developed a hygromorphic double-layered actuator (HDA) by layer-by-layer (LbL) deposition of a poly(allylamine hydrochloride) (PAH) and PAA polyelectrolyte film on one side of a rectangular piece of hydrophobic polytetrafluoroethylene (PTFE) thread tape (**Figure 11**A), for which motion can be controlled by altering the RH of the local environment.[59] PAH and PAA were used for LbL assembly of hygroscopic films because of
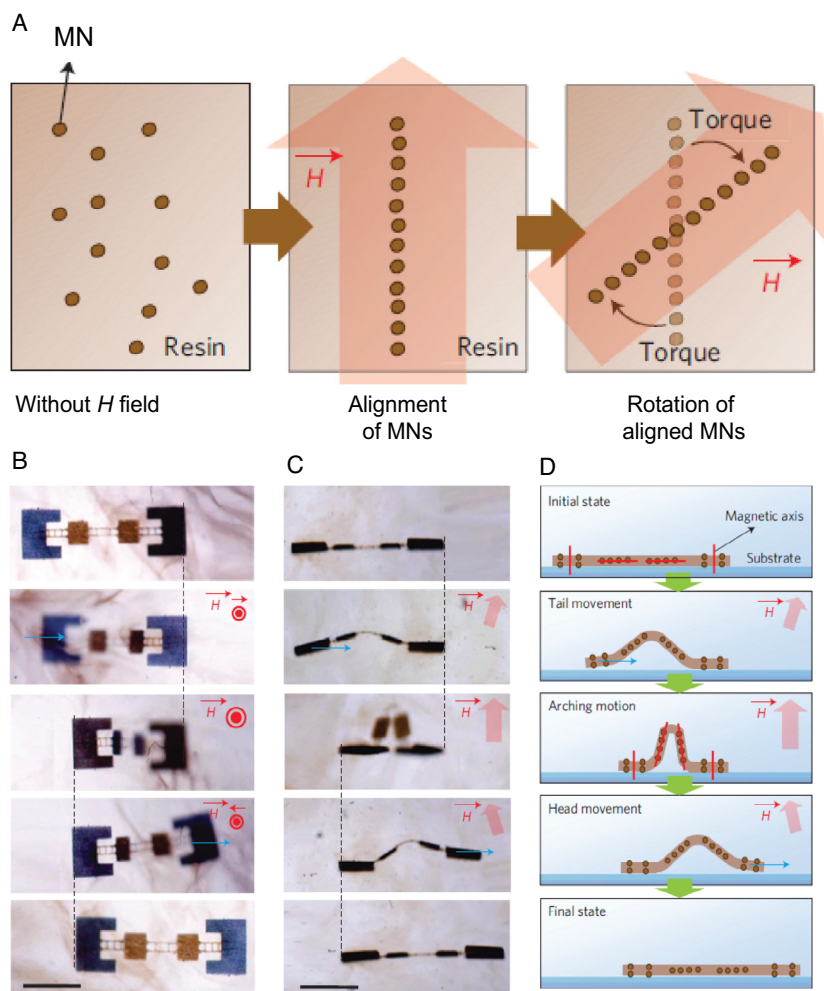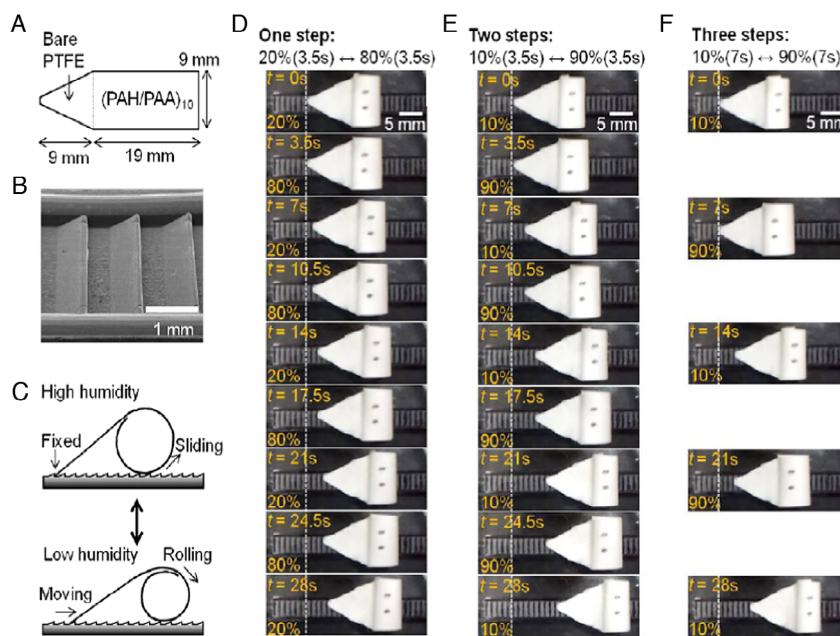
Figure 10. A) Illustration of magnetic nanoparticle self-assembly. Digital photograph of movement of a polymer microlooper in an external magnetic field, B) top view and C) side view. D) Illustration of magnetic-field-triggered actuation of the polymer microlooper. Adapted with permission.[57] Copyright 2011, Macmillan Publishers Limited.

the appreciable water uptake capacity of PAH/PAA films (≈40% of dried film mass at 100% RH) and relative ease of deposition of these films onto nonadhesive surfaces. The locomotion of the actuator can be precisely controlled by changing the duration of cycles of humidity exposure and RH, which control the swelling of the LbL layers. The HDA actuator consists of a PTFE ribbon with a rectangular section on it coated with ten bilayers (BL) of a PAH/PAA film (equivalent to 190 nm in thickness on a silicon wafer) and a tapered region with bare PTFE forming the tail. When exposed to cycles of high (≥80%) and low (≤20%) RH, the PAH/PAA-coated region coils up to form the head of the HDA. When exposed to high RH, swelling of the PAH/PAA film increases the radius of the coiled head, moving the center of mass of the HDA along the head direction, sliding the head forward on the track. Reducing the RH decreases the radius of the head such that the head recoils and rolls on the track dragging the tail forward. This dragging motion moves the center of mass of the HDA forward (Figure 11C–F). The time required for swelling and deswelling of the PAH/PAA LbL films on varying the RH from 20% to 80% and from 80% to 20% are 2.8 and 8.0 s,

respectively. The step length of the HDA was found to decrease with increase in absolute values of RH. The step length can be described as the number of steps of the ratchet track travelled by the HDA during one cycle of high and low RH exposure. The step length increased with longer exposure time and larger difference between low and high RH. At the same time, the step length was found to be linearly proportional to the thickness of the PAH/PAA film.

As these devices operate on minute fluctuations in environmental conditions, they can be used to fabricate low-power-consumption actuators. Another interesting humidity-sensitive actuator film composed of a π–π stacked carbon nitride polymer (CNP) was serendipitously discovered by Aida and coworkers while working with guanidinium carbonate (Gdm$_2$CO$_3$).[60] This CNP-based actuator film undergoes very fast actuating motion triggered by a minute amount of water (several hundred nanograms per 10 mm^2 of surface area), which any conventional hygrometer would fail to detect. They found that calcination of Gdm$_2$CO$_3$ in a test tube deposited a yellowish transparent film on the upper inner surface of the tube along with a yellowish

ADVANCED
SCIENCE NEWS
www.advancedsciencenews.com

ADVANCED
INTELLIGENT
SYSTEMS
Open Access

www.advintellsyst.com

Figure 11. A) Design of an HDA showing a PAH/PAA-coated head and a bare PTFE tail. B) Scanning electron microscope image of the ratchet track with a step size of ≈1 mm. C) Diagram showing movement of the HDA on the ratchet track. D–F) Digital photographs showing locomotion of the HDA on exposure to high and low RH. Adapted with permission.[59] Copyright 2013, American Chemical Society.

powdery substance at the bottom. Structural analysis revealed that both the transparent film and the powdery substance are CNPs in which heptazine forms the repeating unit. Thus, an ≈0.8 μm thin CNP film was formed on the glass substrate by one-pot vapor deposition polymerization on thermal decomposition of Gdm_2CO_3. The film was detached from the glass surface by soaking in hot water at 70 °C. The thickness of the film could be changed by varying the amount of Gdm_2CO_3 and the heating time. The fundamental working principle is similar to that of the previously described system. The CNP desorbs water at low levels of humidity, experiencing a bending motion toward the growing surface of the film, whereas at high levels of humidity adsorption of water takes place and the CNP film straightens, though the mechanism at the molecular level can be explained taking the ratio of unreacted sp^3 nitrogen to sp^2 nitrogen along the thickness of the polymer film into consideration. The CNP film formed was nonsymmetric along the thickness (**Figure 12**A) and had larger plane-to-plane separation, i.e., structurally less ordered as well as a larger number of unreacted NH_2 groups on its growth side compared to the substrate side. Polarized attenuated total reflectance Fourier transform infrared (ATR-FTIR) spectroscopy revealed that the unreacted NH_2 groups of the polymer were oriented horizontally to the plane of the film and adsorbed a large number of water molecules on the growth side of the film under moist conditions. Large contractile strain produced on the growth side as a result of water adsorption caused the film to bend to the growth side (Figure 12B). Due to the hydrophobic nature of the CNP film, water molecules remained only at the surface bonded to the unreacted amino groups and did not penetrate deep into the bulk. As a consequence of rapid surface adsorption and desorption, the polymer film demonstrated ultrafast actuating motion under negligible

fluctuations in humidity. Because adsorption/desorption of water molecules can be achieved by regulating the temperature, the actuating motion can be produced at constant humidity. In addition, the CNP film underwent a quick bending motion on irradiation with UV light. The actuating motion of the film under UV irradiation was possibly due to adsorption/desorption of water molecules from the surface due to the photothermal effect. The CNP film underwent more than 10 000 reversible bending/straightening motions when irradiated with a UV lamp which was programmed to flash at an interval of 0.1 s over a period of 5 h with an interval of 1.9 s. To fabricate a film actuator that would demonstrate unidirectional walking, a hybrid CNP film was developed by depositing a 120 nm thick gold film onto half of the film on its growth side (Figure 12C). It is worth mentioning that this partial protection against water adsorption facilitated unidirectional walking. In addition, the actuator walked faster when in proximity of a water droplet (Figure 12D).

2.6. Self-Oscillating Reaction-Driven Actuators

The Belouzov–Zhabotinsky (BZ) reaction can generate periodic swelling–deswelling oscillations in polymer gels by converting the chemical energy from the reaction into mechanical oscillations and is a special type of trigger used in shape memory actuators. The BZ reaction is catalyzed by a ruthenium catalyst covalently attached to the polymer chains. Periodic change in the oxidation state of the ruthenium catalyst during the reaction alters the hydrophilicity of the polymers and drives the rhythmic swelling/deswelling of the gel network. A poly(NIPAM-co-Ru(bpy)$_3$-co-AMPS)-based hydrogel actuator undergoes autonomous asymmetric swelling–deswelling oscillations fuelled by the BZ reaction (**Figure 13**) when immersed in a solution
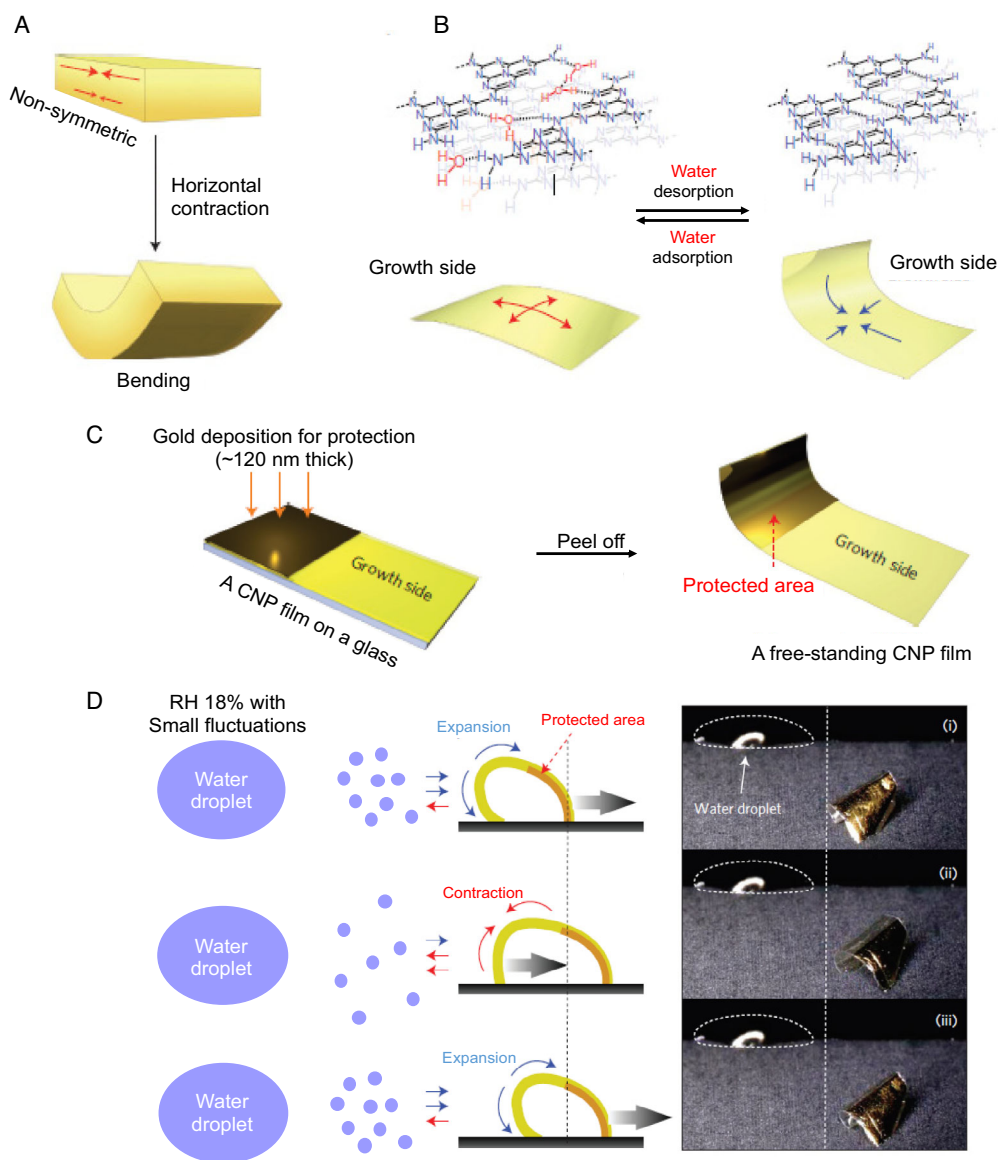
Figure 12. A) Schematic representations of contraction of nonsymmetric film. B) Mechanism demonstrating bending and straightening of CNP film due to desorption/adsorption of water, respectively. C) Illustration of preparation of a gold-protected (partially) CNP film. D) Schematic representation and photographs showing unidirectional "walk" of a partially protected CNP film in the presence of a water droplet. Adapted with permission.[60] Copyright 2016, Macmillan Publishers Limited.

containing BZ substrates (62.5 mM malonic acid, 84 mM sodium bromate, and 0.894 M nitric acid)[61] The BZ reaction takes place inside the gel matrix after the substrate penetrates the network. Higher charge density in the oxidized state of the catalyst increases the LCST of the polymer. Consequently, changes in redox state result in periodical swelling and deswelling of the gel. The monomer solution was polymerized by free radical polymerization in a mold consisting of a hydrophilic glass plate and hydrophobic teflon plate separated by silicon rubber (0.5 mm thick) as spacer. $Ru(bpy)_3^{2+}$ being hydrophobic migrates toward the Teflon surface, whereas AMPS being hydrophilic migrates to the glass surface, creating a concentration gradient along the thickness direction. The swelling ratio of the gel membrane in water is larger at the side with a higher concentration of hydrophilic AMPS than in the opposite side, where the concentration of hydrophobic $Ru(bpy)_3^{2+}$ is higher. As a result, the gel strip always bends in the direction of the hydrophobic $Ru(bpy)_3^{2+}$. The bending and stretching were translated to a one-directional motion using an asymmetrical ratchet surface made of acrylic sheet as the rough surface for walking. Repeated bending and stretching motion on the ratchet surface results in forward motion of the gel, the teeth of the ratchet preventing the walker from sliding backward. Results showed that a walking velocity of $\approx 170 \, \mu m \, min^{-1}$ could be attained for this system. Very useful from the application point of view, the walking velocity can be regulated by changing the concentration of the substrate.
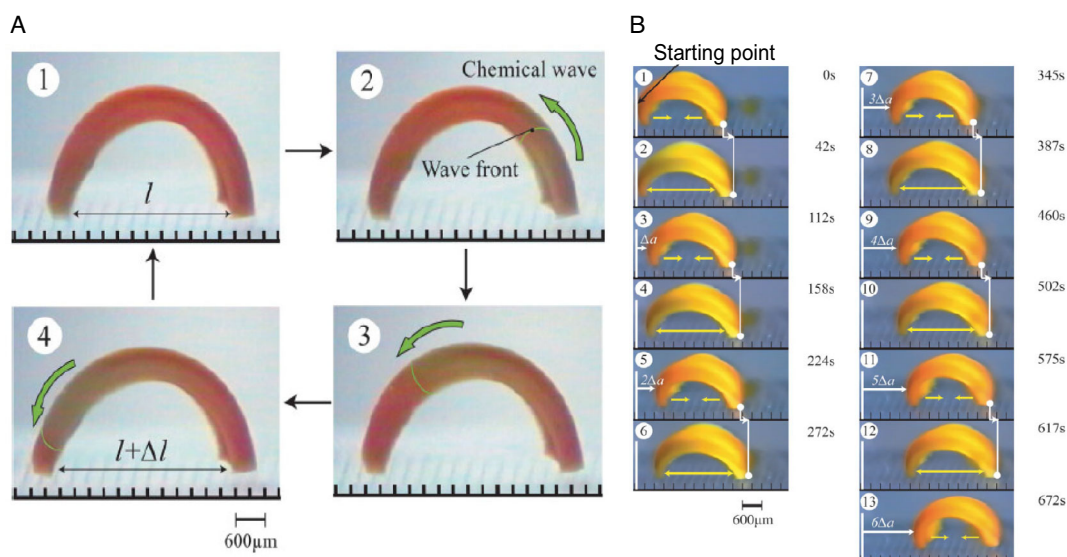
Figure 13. A) Images showing reversible bending–stretching of poly(NIPAM-*co*-Ru(bpy)$_3$-*co*-AMPS) hydrogel due to propagation of a chemical wave (generated from an oscillating chemical reaction occurring within the gel) from one edge to the other. B) Digital photograph of "self-walking" motion of the actuator. Adapted with permission.[61] Copyright 2007, John Wiley & Sons.

Self-propelled actuation in BZ gels can also be regulated by a cross-link density gradient in their network along the thickness of the gel, which leads to oscillatory bending and straightening of the gel network. Structural heterogeneity can be introduced by photo-crosslinking the monomer with UV light from one side of the glass capillary in which the monomer solution is taken.[62] [Ru(bpy)$_3$]$^{2+}$, which acts the catalyst for the BZ reaction, absorbs the incident UV light and so the intensity of light penetrating the solution decreases with depth, and accordingly the cross-linking density decreases along the gel thickness direction. Consequently, the pore size of the gel network increases gradually from the side of the gel photoirradiated throughout the thickness. When this gel was immersed into a BZ substrate solution, the linear gel showed periodic bending and unbending. Both experimental studies and simulations showed that average degree of bending increased with time. The self-walking actuator described in this work is clearly a potential candidate for artificial muscles or biomimetic robots that require autonomous motion.

3. Conclusions

In summary, we have presented an account of some of the latest progress in the field of shape memory actuators that can display controllable unidirectional movements. The fundamental working principle of each polymer system, the conditions required to trigger the actuating behavior, the type of molecular switch used along with its intrinsic susceptibility, and the response of the polymer have been discussed. After careful analysis of the systems, it can be concluded that anisotropy or inhomogeneous structure is the key feature to achieve specific control over the shape deformation. Various shape deformations such as bending, folding stretching, expansion/contraction, and arching could be achieved by constructing bilayer, patterned, gradient, and other anisotropic structures. It is important to emphasize that
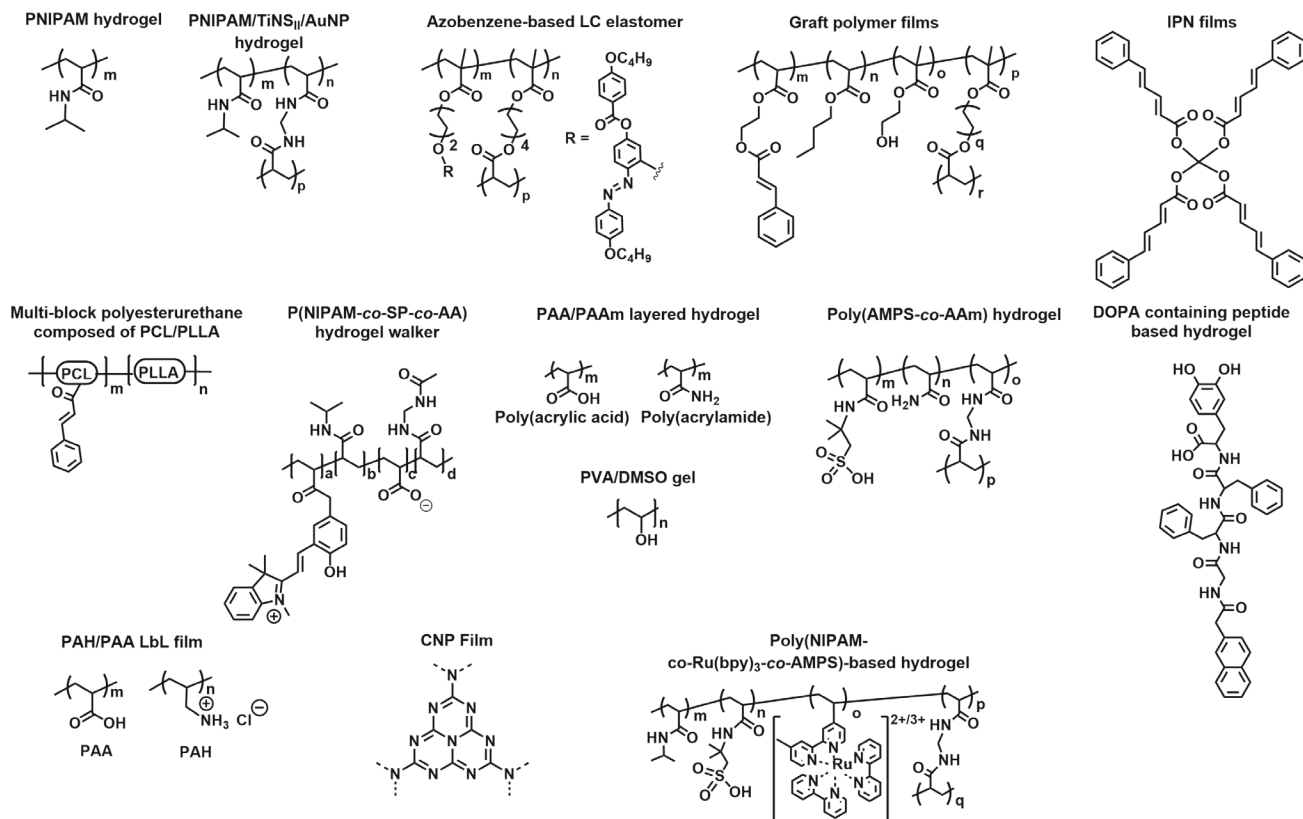
unidirectional movement in shape memory actuators has been realized by coordinated execution of two or more of these simple shape deformations by a single system. Furthermore, the actuating movements of these existing shape memory actuators have all been demonstrated only at the laboratory scale.

Nevertheless, for real-life applications there are some common challenges that need to be addressed for developing efficient actuators displaying unidirectional movement. For instance, hydrogel-based walkers require an aqueous medium to carry out the actuation, because the mechanism of operation involves transfer of water between the hydrogel matrix and the surrounding medium regardless of the trigger. As a possible alternative, stimulus-responsive hydrogel that shows actuating behavior in open air by means of water exchange with air has been developed and investigated, but the performance of such devices in terms of the shape deformation extent, distance walked, and response rate is not yet adequate. For hydrogel actuators, additional constraints are given by poor mechanical properties, which can be improved by incorporating organic or inorganic additives into the hydrogel matrix. Precise control over shape deformation is also essential, and for that purpose actuators with inhomogeneous structures should be fabricated by techniques such as 3D printing to have better control over the actuating behaviors. Furthermore, a higher number of devices that respond to a magnetic field or light are still needed to make noncontact operations possible, which will have potential applications in the area of active medical devices. Finally, to widen the application scope it is necessary to focus our attention during the next years toward the development of low-cost, reproducible, and scalable shape memory actuators with tunable multistimuli sensitivity and unidirectional motion.

Appendix A

Relevant chemical structures associated with Table 1.

ADVANCED
SCIENCE NEWS

www.advancedsciencenews.com

ADVANCED
INTELLIGENT
SYSTEMS
Open Access

www.advintellsyst.com

PNIPAM hydrogel

PNIPAM/TiNS$_{II}$/AuNP hydrogel

Azobenzene-based LC elastomer

Graft polymer films

IPN films

Multi-block polyesterurethane composed of PCL/PLLA

P(NIPAM-co-SP-co-AA) hydrogel walker

PAA/PAAm layered hydrogel

Poly(acrylic acid)   Poly(acrylamide)

PVA/DMSO gel

Poly(AMPS-co-AAm) hydrogel

DOPA containing peptide based hydrogel

PAH/PAA LbL film

PAA   PAH

CNP Film

Poly(NIPAM-co-Ru(bpy)$_3$-co-AMPS)-based hydrogel

Conflict of Interest

The authors declare no conflict of interest.

[1] Y. Osada, H. Okuzaki, H. Hori, *Nature* **1992**, *355*, 242.

[2] X. Le, W. Lu, J. Zhang, T. Chen, *Adv. Sci.* **2019**, *6*, 1801584.

[3] Q. Shi, H. Liu, D. Tang, Y. Li, X. Li, F. Xu, *NPG Asia Materials* **2019**, *11*, 1.

[4] A. Lendlein, S. Kelch, *Angew. Chem., Int. Ed.* **2002**, *41*, 2034.

[5] H. Ko, A. Javey, *Acc. Chem. Res.* **2017**, *50*, 691.

[6] M. P. M. Dicker, A. B. Baker, R. J. Iredale, S. Naficy, I. P. Bond, C. F. J. Faul, J. M. Rossiter, G. M. Spinks, P. M. Weaver, *Sci. Rep.* **2017**, *7*, 9197.

[7] J. J. Wu, Y. T. Lin, J. Z. Sun, *J. Mater. Chem.* **2012**, *22*, 17449.

[8] A. Lendlein, R. Langer, *Science* **2002**, *296*, 1673.

[9] H. Zeng, O. M. Wani, P. Wasylczyk, R. Kaczmarek, A. Priimagi, *Adv. Mater.* **2017**, *29*, 1701814.

[10] T. Shen, M. G. Font, S. Jung, M. L. Gabriel, M. P. Stoykovich, F. J. Vernerey, *Sci. Rep.* **2017**, *7*, 1.

[11] J. Shang, X. Le, J. Zhang, T. Chen, P. Theato, *Polym. Chem.* **2019**, *10*, 1036.

[12] H. Xiao, C. Ma, X. Le, L. Wang, W. Lu, P. Theato, T. Hu, J. Zhang, T. Chen, *Polymers* **2017**, *9*, 138.

[13] B. Maiti, A. Abramov, L. Franco, J. Puiggalí, H. Enshaei, C. Aleman, D. D. Díaz, *Adv. Func. Mater.* **2020**, *30*, 2001683.

[14] T. Koga, K. Tomimori, N. Higashi, *Macromol. Rapid Commun.* **2020**, *1900650*, 41.

[15] Z. Liu, R. Tang, D. Xu, J. Liu, H. Yu, *Macromol. Rapid Commun.* **2015**, *36*, 1171.

[16] X. Le, W. Lu, H. Xiao, L. Wang, C. Ma, J. Zhang, Y. Huang, T. Chen, *ACS Appl. Mater. Interfaces* **2017**, *9*, 9038.

[17] N. Bassik, B. T. Abebe, K. E. Laflin, D. H. Gracias, *Polymer* **2010**, *51*, 6093.

[18] C. Yang, Z. Liu, C. Chen, K. Shi, L. Zhang, X.-J. Ju, W. Wang, R. Xie, L.-Y. Chu, *ACS Appl. Mater. Interfaces* **2017**, *9*, 15758.

[19] X. Yu, S. Zhou, X. Zheng, T. Guo, Y. Xiao, B. Song, *Nanotechnology* **2009**, *20*, 235702.

[20] J. M. Rochette, V. S. Ashby, *Macromolecules* **2013**, *46*, 2134.

[21] C. Ma, W. Lu, X. Yang, J. He, X. Le, L. Wang, J. Zhang, M. J. Serpe, Y. Huang, T. Chen, *Adv. Funct. Mater.* **2018**, *28*, 1704568.

**ADVANCED
SCIENCE NEWS**

www.advancedsciencenews.com

**ADVANCED
INTELLIGENT
SYSTEMS**
Open Access

www.advintellsyst.com

[22] Y. Yao, J. T. Waters, A. V. Shneidman, J. Cui, X. Wang, N. K. Mandsberg, S. Lia, A. C. Balazs, J. Aizenberg, *Proc. Natl. Acad. Sci. USA* **2018**, *115*, 12950.

[23] A. Katchalsky, M. Zwick, *J. Polym. Sci.* **1955**, *16*, 221.

[24] W. Kuhn, B. Hargitay, A. Katchalsky, H. Eisenberg, *Nature* **1950**, *165*, 514.

[25] Y. Yu, T. Ikeda, *Angew. Chem., Int. Ed.* **2006**, *45*, 5416.

[26] X. Li, S. Ma, J. Hu, Y. Ni, Z. Lin, H. Yu, *J. Mater. Chem. C*, **2019**, *7*, 622.

[27] I. K. Han, T. Chung, J. Han, Y. S. Kim, *Nano Converg.* **2019**, *6*, 1.

[28] C. Liu, H. Qin, P. Mather, *J. Mater. Chem.* **2007**, *17*, 1543.

[29] M. Moniruzzman, K. I. Winey, *Macromolecules* **2006**, *39*, 5194.

[30] X.-X. Le, Y.-C. Zhang, W. Lu, L. Wang, J. Zheng, I. Ali, J.-W. Zhang, Y.-J. Huang, M. J. Serpe, X.-T. Yang, X.-D. Fan, T. Chen, *Macromol. Rapid Commun.* **2018**, *39*, 1800019.

[31] Y. Takashima, S. Hatanaka, M. Otsubo, M. Nakahata, T. Kakuta, A. Hashidzume, H. Yamaguchi, A. Harada, *Nat. Commun.* **2012**, *3*, 1.

[32] Z. L. Wu, M. Moshe, J. Greener, H. Therien-Aubin, Z. H. Nie, E. Sharon, E. Kumacheva, *Nat. Commun.* **2013**, *4*, 1586.

[33] J. Hu, X. Li, Y. Ni, S. Ma, H. Yu, *J. Mater. Chem. C* **2018**, *6*, 10815.

[34] O. Erol, A. Pantula, W. Liu, D. H. Gracias, *Adv. Mater. Technol.* **2019**, *4*, 1900043.

[35] H. Banerjee, Md. Suhail, H. Ren, *Biomimetics* **2018**, *3*, 15.

[36] L. Yeghiazarian, S. Mahajan, C. Montemagno, C. Cohen, U. Wiesner, *Adv. Mater.* **2005**, *17*, 1869.

[37] G. Stoychev, N. Puretskiy, L. Ionov, *Soft Matter* **2011**, *7*, 3277.

[38] Y. S. Kim, M. Liu, Y. Ishida, Y. Ebina, M. Osada, T. Sasaki, T. Hikima, M. Takata, T. Aida, *Nat. Mater.* **2015**, *14*, 1002.

[39] P. Calvert, *MRS Bull.* **2008**, *33*, 207.

[40] M.-H. Li, P. Keller, B. Li, X. Wang, M. Bruner, *Adv. Mater.* **2003**, *15*, 569.

[41] A. H. Gelebart, D. J. Mulder, M. Varga, A. Konya, G. Vantomme, E. W. Meijer, R. L. B. Selinger, D. J. Broer, *Nature* **2017**, *546*, 632.

[42] A. Lendlein, H. Jiang, O. Jünger, R. Langer, *Nature* **2005**, *434*, 879.

[43] L. Wu, C. Jin, X. Sun, *Biomacromolecules* **2011**, *12*, 235.

[44] X. Lu, S. Guo, X. Tong, H. Xia, Y. Zhao, *Adv. Mater.* **2017**, *29*, 1606467.

[45] W. Francis, A. Dunne, C. Delaney, L. Florea, D. Diamond, *Sens. Actuators B* **2017**, *250*, 608.

[46] S. Ma, X. Li, S. Huang, J. Hu, H. Yu, *Angew. Chem.* **2019**, *131*, 2681.

[47] M. Yamada, M. Kondo, R. Miyasato, Y. Naka, J. Mamiya, M. Kinoshita, A. Shishido, Y. Yu, C. J. Barrett, T. Ikeda, *J. Mater. Chem.* **2009**, *19*, 60.

[48] Z. Sun, Y. Yamauchi, F. Araoka, Y. S. Kim, J. Bergueiro, Y. Ishida, Y. Ebina, T. Sasaki, T. Hikima, T. Aida, *Angew. Chem., Int. Ed.* **2018**, *57*, 15772.

[49] C. Wu, J. Feng, L. Peng, Y. Ni, H. Liang, L. He, Y. Xie, *J. Mater. Chem.* **2011**, *21*, 18584.

[50] Z. Li, Y. Yang, Z. Wang, X. Zhang, Q. Chen, X. Qian, N. Liu, Y. Wei, Y. Ji, *J. Mater. Chem. A* **2017**, *5*, 6740.

[51] H. Tian, Z. Wang, Y. Chen, J. Shao, T. Gao, S. Cai, *ACS Appl. Mater. Interfaces* **2018**, *10*, 8307.

[52] Z. Liu, P. Calvert, *Adv. Mater.* **2000**, *12*, 288.

[53] S. Liang, J. Xu, L. Weng, L. Zhang, X. Guo, X. Zhang, *J. Phys. Chem. B* **2007**, *111*, 941.

[54] C. Yang, W. Wang, C. Yao, R. Xie, X.-J. Ju, Z. Liu, L.-Y. Chu, *Sci. Rep.* **2015**, *5*, 1.

[55] D. Morales, E. Palleau, M. D. Dickey, O. D. Velev, *Soft Matter* **2014**, *10*, 1337.

[56] B. Xue, M. Qin, T. Wang, J. Wu, D. Luo, Q. Jiang, Y. Li, Y. Cao, W. Wang, *Adv. Funct. Mater.* **2016**, *26*, 9053.

[57] J. Kim, S. E. Chung, S.-E. Choi, H. Lee, J. Kim, S. Kwon, *Nat. Mater.* **2011**, *10*, 747.

[58] W. Hu, G. Z. Lum, M. Mastrangeli, M. Sitti, *Nature* **2018**, *554*, 81.

[59] S.-W. Lee, J. H. Prosser, P. K. Purohit, D. Lee, *ACS Macro Lett.* **2013**, *2*, 960.

[60] H. Arazoe, D. Miyajima, K. Akaike, F. Araoka, E. Sato, T. Hikima, M. Kawamoto, T. Aida. *Nat. Mater.* **2016**, *15*, 1084.

[61] S. Maeda, Y. Hara, T. Sakai, R. Yoshida, S. Hashimoto, *Adv. Mater.* **2007**, *19*, 3480.

[62] O. Kuksenok, V. V. Yashin, M. Kinoshita, T. Sakai, R. Yoshida, A. C. Balazs, *J. Mater. Chem.* **2011**, *21*, 8360.

Mridula Nandi obtained her B.Sc. degree in chemistry in 2013 from the University of Calcutta, India. In 2015, she completed her master's thesis on the preparation and characterization of hydrogels at IISER Kolkata. She continued there her Ph.D. work on synthesis and applications of different polymeric architectures under the supervision of Dr. Priyadarsi De. She is currently a postdoctoral researcher in the group of Prof. Díaz working on actuators for biomedicine.

Binoy Maiti received his B.Sc. degree in chemistry in 2010 from the University of Calcutta, India. He obtained his M.Sc. degree in organic chemistry in 2012 from the same university. He received his Ph.D. degree under the supervision of Dr. Priyadarsi De (IISER Kolkata). He worked on the synthesis of fatty acid–based polymers using controlled polymerization techniques. He is currently a postdoctoral researcher in the group of Prof. Díaz working on stimuli-responsive materials.

David Díaz received his Ph.D. in chemistry from the University of La Laguna (ULL) (2002). Then, he joined Prof. Finn's group at TSRI, USA. Since 2006, he has held positions in academia and industry (Ramón y Cajal, UAM, Spain, 2006; Dow, Switzerland, 2007; CSIC, Spain, 2009; University of Regensburg, Germany: Alexander von Humboldt Researcher (2010), Heisenberg Professor (2013), Privatdozent (2018)). In 2020, he was appointed as Distinguished Researcher (ULL). His research focuses on functional materials.